



Denitrification, dehydration and ozone loss during the 2015/2016 Arctic winter

Farahnaz Khosrawi¹, Oliver Kirner², Björn-Martin Sinnhuber¹, Sören Johansson¹, Michael Höpfner¹, Michelle L. Santee³, Lucien Froidevaux³, Jörn Ungermann⁴, Roland Ruhnke¹, Wolfgang Woiwode¹, Hermann Oelhaf¹, and Peter Braesicke¹

¹Institute of Meteorology and Climate Research, Karlsruhe Institute of Technology, Karlsruhe, Germany

²Steinbuch Centre for Computing, Karlsruhe Institute of Technology, Karlsruhe, Germany

³Jet Propulsion Laboratory, California Institute of Technology, Pasadena, CA, USA

⁴Institute of Energy and Climate Research, Forschungszentrum Jülich, Jülich, Germany

Correspondence to: Farahnaz Khosrawi (farahnaz.khosrawi@kit.edu)

Received: 29 May 2017 – Discussion started: 8 June 2017

Revised: 14 September 2017 – Accepted: 27 September 2017 – Published: 1 November 2017

Abstract. The 2015/2016 Arctic winter was one of the coldest stratospheric winters in recent years. A stable vortex formed by early December and the early winter was exceptionally cold. Cold pool temperatures dropped below the nitric acid trihydrate (NAT) existence temperature of about 195 K, thus allowing polar stratospheric clouds (PSCs) to form. The low temperatures in the polar stratosphere persisted until early March, allowing chlorine activation and catalytic ozone destruction. Satellite observations indicate that sedimentation of PSC particles led to denitrification as well as dehydration of stratospheric layers. Model simulations of the 2015/2016 Arctic winter nudged toward European Centre for Medium-Range Weather Forecasts (ECMWF) analysis data were performed with the atmospheric chemistry–climate model ECHAM5/MESSy Atmospheric Chemistry (EMAC) for the Polar Stratosphere in a Changing Climate (POLSTRACC) campaign. POLSTRACC is a High Altitude and Long Range Research Aircraft (HALO) mission aimed at the investigation of the structure, composition and evolution of the Arctic upper troposphere and lower stratosphere (UTLS). The chemical and physical processes involved in Arctic stratospheric ozone depletion, transport and mixing processes in the UTLS at high latitudes, PSCs and cirrus clouds are investigated. In this study, an overview of the chemistry and dynamics of the 2015/2016 Arctic winter as simulated with EMAC is given. Further, chemical–dynamical processes such as denitrification, dehydration and ozone loss during the 2015/2016 Arctic winter are investigated. Compar-

isons to satellite observations by the Aura Microwave Limb Sounder (Aura/MLS) as well as to airborne measurements with the Gimbalbed Limb Observer for Radiance Imaging of the Atmosphere (GLORIA) performed aboard HALO during the POLSTRACC campaign show that the EMAC simulations nudged toward ECMWF analysis generally agree well with observations. We derive a maximum polar stratospheric O₃ loss of ~ 2 ppmv or 117 DU in terms of column ozone in mid-March. The stratosphere was denitrified by about 4–8 ppbv HNO₃ and dehydrated by about 0.6–1 ppmv H₂O from the middle to the end of February. While ozone loss was quite strong, but not as strong as in 2010/2011, denitrification and dehydration were so far the strongest observed in the Arctic stratosphere in at least the past 10 years.

1 Introduction

Since the early 1980s (thus, for more than 30 years), substantial ozone depletion has been observed each year during winter and spring in the Antarctic stratosphere (WMO, 2010). Polar ozone depletion is associated with enhanced chlorine from anthropogenic chlorofluorocarbons and heterogeneous chemistry under cold conditions. The deep Antarctic “hole” contrasts with the generally weaker ozone depletion observed in the warmer Arctic (Solomon et al., 2014). Nevertheless, substantial ozone depletion has been observed for cold Arctic winters. Especially, in the past 15 years, ozone loss in the Arctic occasionally approached the degree of

ozone loss in the Antarctic in, e.g. winter 2004/2005 (e.g. Manney et al., 2006; Tilmes et al., 2006; Livesey et al., 2015, and references therein) and 2010/2011 (e.g. Manney et al., 2011; Sinnhuber et al., 2011; Hommel et al., 2014).

Polar stratospheric clouds (PSCs) play a key role in stratospheric ozone destruction in the polar regions (Solomon et al., 1986; Crutzen and Arnold, 1986). Heterogeneous reactions which take place on and within the PSC particles convert halogens from relatively inert reservoir species into forms which can destroy ozone in the polar spring (e.g. Peter, 1997; Solomon, 1999; Lowe and MacKenzie, 2008). PSCs form at altitudes between 15 and 30 km and consist of liquid and/or solid particles. According to their composition and physical state, they have been classified into three different types: (1) supercooled ternary solution (STS), (2) nitric acid trihydrate (NAT) and (3) water ice. Liquid PSC cloud particles (STS) form by the condensation of water vapour (H_2O) and nitric acid (HNO_3) on the liquid stratospheric background sulfate aerosol particles at temperatures 2–3 K below the NAT existence temperature T_{NAT} (~ 195 K at 50 hPa), while for the formation of solid cloud particles (NAT and ice) lower temperatures are required (slightly above or below the ice frost point $T_{\text{ice}} \sim 188$ K at 50 hPa) (e.g. Carslaw et al., 1994; Koop et al., 1995).

Solid PSC particles can grow to larger sizes than liquid PSC particles and finally sediment out of the stratosphere (Fahey et al., 2001). The sedimentation of the solid particles can lead to dehydration and/or denitrification of the stratosphere. Solid HNO_3 containing PSC particles leading to denitrification can either consist of NAT or ice depending on the prevailing formation mechanism. It has been shown that the nucleation of NAT on ice is quite efficient (e.g. Fueglistaler et al., 2002; Hoyle et al., 2013). The sedimentation of large HNO_3 containing ice PSC particles can lead to greater denitrification than the sedimentation of (typically smaller) NAT or liquid PSC particles alone (Lowe and MacKenzie, 2008; Wohltmann et al., 2013; Manney and Lawrence, 2016).

Denitrification limits the deactivation process of the ozone-destroying substances in springtime and thus leads to a prolongation of the ozone-destroying cycles (e.g. Salawitch et al., 1993; Rex et al., 1997). Evidence of denitrification has been found in the Arctic and Antarctic from in situ and remote sensing observations (Fahey et al., 1990; Solomon, 1999; Waibel et al., 1999; Kondo et al., 2000; Santee et al., 2000; Manney et al., 2011). Denitrification is most intense over the Antarctic region, where large fractions of available NO_y are irreversibly removed from the stratosphere each winter. NO_y is the sum of principal reactive nitrogen species, of which HNO_3 , NO , NO_2 , N_2O_5 and ClONO_2 are important in the lower stratosphere (Fahey et al., 1989). Dehydration in the stratosphere is generally observed over the Antarctic (e.g. Kelly et al., 1989; Vömel et al., 1995; Nedoluha et al., 2000) but only rarely in the Arctic (e.g. Fahey et al., 1990; Vömel et al., 1997; Pan et al., 2002; Schiller et al., 2002; Khaykin et al., 2013).

Another factor contributing to the severity of polar ozone destruction is the reduction of nitrogen ($\text{NO}_x = \text{NO} + \text{NO}_2$) via the conversion of NO_x into HNO_3 on the surfaces of PSCs, known as denoxification. Denoxification becomes important if temperatures are continuously low during the course of the winter as is the case in the Antarctic (e.g. Waibel et al., 1999). It has been shown that polar vortex stability, chlorine activation and ozone loss tend to be greater with lower vortex temperatures (e.g. von Hobe et al., 2013). Therefore, it is not surprising that the most severe ozone loss ever observed in the Arctic occurred in spring 2011, at the end of the most persistently cold Arctic winter in the stratosphere on record (Manney et al., 2011; Sinnhuber et al., 2011; Hommel et al., 2014).

The 2015/2016 Arctic winter was one of the coldest stratospheric winters in recent years. Indeed, the Arctic polar vortex in the early winter 2015/2016 was the strongest and coldest of the last 68 years (Matthias et al., 2016). Temperatures within the vortex dropped below T_{NAT} , thus allowing PSCs to form. Tropospheric and stratospheric cloud structures were observed simultaneously over Svalbard. Synoptic-scale PSCs extended over a nearly 8 km deep layer (Dörnbrack et al., 2017). The low temperatures in the polar stratosphere persisted until early March, allowing PSC formation, chlorine activation and catalytic ozone destruction. Satellite observations indicate that sedimentation of PSC particles led to denitrification as well as dehydration of stratospheric layers (Manney and Lawrence, 2016). Widespread persistent ice PSC layers were observed by the Cloud-Aerosol Lidar and Infrared Pathfinder Satellite Observations (CALIPSO) (Voigt et al., 2016). Ozone destruction was strong, but not as strong as in 2010/2011, since a major final sudden stratospheric warming ended the 2015/2016 Arctic winter by early March (Manney and Lawrence, 2016).

Model simulations of the 2015/2016 Arctic winter nudged toward European Centre for Medium-Range Weather Forecasts (ECMWF) analysis were performed with the atmospheric chemistry–climate model ECHAM5/MESy Atmospheric Chemistry (EMAC) for the POLSTRACC (Polar Stratosphere in a Changing Climate) campaign. POLSTRACC was a HALO (High Altitude and Long Range Research Aircraft) mission aiming at the investigation of the structure, composition and evolution of the Arctic upper troposphere lower stratosphere (UTLS). The chemical and physical processes involved in Arctic stratospheric ozone depletion, transport and mixing processes in the UTLS at high latitudes, PSCs and cirrus clouds were investigated. In this study, an overview of the chemistry and dynamics of the 2015/2016 Arctic winter as simulated with EMAC is given. Chemical–dynamical processes such as denitrification, dehydration and ozone loss will be investigated and comparisons to satellite observations by the Aura Microwave Limb Sounder (Aura/MLS) as well as to airborne measurements with the Gimbalbed Limb Observer for Radiance Imaging of

the Atmosphere (GLORIA) performed aboard HALO will be shown.

2 Model simulations and observations

2.1 EMAC

The ECHAM5/MESSy Atmospheric Chemistry (EMAC) model is a numerical chemistry and climate simulation system that includes submodels describing tropospheric and middle atmospheric processes and their interaction with oceans, land and human influences (Jöckel et al., 2010). It uses the second version of the Modular Earth Submodel System (MESSy2) to link multi-institutional computer codes. The core atmospheric model is the fifth-generation European Centre Hamburg general circulation model (ECHAM5; Roeckner et al., 2006). For the present study, we applied EMAC (ECHAM5 version 5.3.02, MESSy version 2.52) in T106L90MA and T42L90MA resolutions, i.e. with a spherical truncation of T106 and T42 (corresponding to a quadratic Gaussian grid of approximately $1.125^\circ \times 1.125^\circ$ and $2.8^\circ \times 2.8^\circ$ degrees, respectively, in latitude and longitude) with 90 vertical hybrid pressure levels from the surface up to 0.01 hPa (approximately 80 km). A Newtonian relaxation technique of the prognostic variables temperature, vorticity, divergence and the (logarithm of the) surface pressure above the boundary layer and below 1 hPa towards ECMWF ERA-Interim reanalysis data (Dee et al., 2011) and ECMWF operational analysis was applied, respectively, in order to nudge the model dynamics towards the observed meteorology.

For the analysis of the 2015/2016 Arctic winter, we used the EMAC data from a T106L90 simulation that was chemically initialised based on a former EMAC simulation. The T106L90 simulation was started on 1 July 2015 and continued until 30 April 2016, applying a nudging toward ECMWF operational analysis. For the comparisons to recent winters, we performed an EMAC T42L90 simulation covering the time period 1 January 2008 to 30 April 2016. The T42L90 simulation was nudged toward ECMWF ERA-Interim analysis data until 30 June 2015 and toward ECMWF operational analysis data thereafter. In both simulations (T106L90 and T42L90), a comprehensive chemistry setup for the stratosphere and troposphere is included. Reaction rate coefficients for gas phase reactions and absorption cross sections for photolysis are taken from Atkinson et al. (2007) and S. P. Sander et al. (2011). The applied model setup was comprised of (among others) the following submodels: MECCA for the gas phase chemistry (R. Sander et al., 2011), JVAL for the calculation of photolysis rates (Sander et al., 2014), MSBM (Multiphase Stratospheric Box Model) for the processes related to PSCs (Kirner et al., 2011), TROPOP for diagnosing the tropopause and boundary layer height, SORBIT for

sampling model data along Sun-synchronous satellite orbits (Jöckel et al., 2010) and H₂O for stratospheric water vapour.

The submodel MSBM simulates the number densities, mean radii and surface areas of sulfuric acid aerosols and liquid and solid PSC particles. The formation of STS particles is calculated according to Carslaw et al. (1995) through the uptake of HNO₃ and H₂O on the liquid binary sulfuric acid/water particles. Ice particles are assumed to form homogeneously at temperatures below T_{ice} . For the simulation of NAT particles, the “kinetic growth NAT parameterisation” is used. The “kinetic” parameterisation is based on the growth and sedimentation algorithm given by Carslaw et al. (2002) and van den Broek et al. (2004). The vapour pressure over ice is calculated according to Marti and Mauersberger (1993) and the vapour pressure over NAT according to Hanson and Mauersberger (1988). NAT formation takes place as soon as a supercooling of 3 K below T_{NAT} is reached. The sedimentation of ice particles is calculated according to Waibel et al. (1999) and for NAT particles according to Carslaw et al. (2002). A total of 11 heterogeneous reactions that occur on the surfaces of liquid and solid PSC particles are considered. A comprehensive description of the submodel MSBM can be found in Kirner et al. (2011).

2.2 Aura/MLS

The Microwave Limb Sounder (MLS) on the Earth Observing System Aura Satellite was launched in July 2004. The Aura/MLS instrument is an advanced successor to the MLS instrument on the Upper Atmosphere Research satellite (UARS). MLS is a limb sounding instrument that measures the thermal emission at millimetre and submillimetre wavelengths using seven radiometers to cover five broad spectral regions (Waters et al., 2006). Measurements are performed from the surface to 90 km with a global latitude coverage from 82° S to 82° N. Vertical profiles are measured every 165 km along the suborbital track with a horizontal resolution of ~ 200 –500 km along track and a footprint of ~ 3 –9 km across track. Here, we use Aura/MLS version 4.2 HNO₃, O₃ and ClO data. The data screening criteria given by Livesey et al. (2017) have been applied to the data.

A detailed assessment of the quality and reliability of the Aura/MLS v2.2 HNO₃ measurements can be found in Santee et al. (2007). The HNO₃ in v3.3 was significantly improved compared to v2.2. In particular, the low bias in the stratosphere was largely eliminated. Measurements of v4.2 HNO₃ are performed with a horizontal resolution of 400–500 km and a vertical resolution of 3–4 km over most of the vertical range. In the lower stratosphere, the precision has been estimated to be 0.6 ppbv and the systematic uncertainty for HNO₃ is estimated to be 0.5–2 ppbv (2σ estimates) (Livesey et al., 2017).

Detailed validation of the MLS O₃ v2.2 product and comparisons with other data sets can be found in Jiang et al. (2007), Froidevaux et al. (2008) and Livesey et al. (2008).

In the stratosphere and above, v4.2 ozone profiles are very similar to the v2.2 and v3.3x/v3.4x profiles. Comparisons have indicated general agreement within 5–10 % with stratospheric profiles from satellite, balloon, aircraft and ground-based data (Livesey et al., 2017).

The quality and reliability of the v2.2 MLS ClO measurements were assessed in detail by Santee et al. (2008). The ClO product was significantly improved in v3.3 and v3.4 (Livesey et al., 2013). In particular, the substantial (~ 0.1 – 0.4 ppbv) negative bias present in the v2.2 ClO values at pressures larger than 22 hPa was mitigated to a large extent, primarily through retrieval of CH_3Cl , which was a new MLS product in v3.3 and v3.4. The ClO retrieval is largely unchanged over much of the profile in v4.2. Measurements of ClO are performed with a horizontal resolution of 300–600 km and a vertical resolution of 3–4.5 km. The precision lies generally within ± 0.1 ppbv (Livesey et al., 2017). Although the negative bias at the lowest retrieval levels has not been entirely eliminated, we make no attempt to correct for it in this analysis.

2.3 GLORIA

The Gimballed Limb Observer for Radiance Imaging of the Atmosphere (GLORIA) combines a classical Fourier transform spectrometer with a 2-D detector array. The instrument takes limb images of the atmosphere from the flight altitude of HALO or M-55 Geophysica down to 4 km. This results in vertical sampling steps of about 150 m at 8 km tangent height from a typical HALO flight level of 14 km. Individual images contain 128 pixels (spectra) in the vertical dimension and 48 pixels in the horizontal dimension. The spectra associated with the pixel rows are binned to reduce uncertainties. The spectral range of the observations currently extends from about 780 to 1400 cm^{-1} (Riese et al., 2014). The list of species with signatures in this spectral range includes temperature, H_2O , HDO , O_3 , CH_4 , N_2O , CFC-11, CFC-12, HCFC-12, SF_6 , HNO_3 , N_2O_5 , ClONO_2 , HO_2NO_2 , PAN, C_2H_6 , H_2CO and NH_3 . Details on the instrument design and calibration are given in Friedl-Vallon et al. (2014) and Kleinert et al. (2014). GLORIA is operated in a high-spectral, medium-spatial sampling (“chemistry”) mode and a medium-spectral, high-spatial sampling (“dynamics”) mode. The spectral samplings are 0.0625 cm^{-1} for the chemistry mode and 0.625 cm^{-1} for the dynamics mode (Riese et al., 2014). In this study, trace gas retrievals from measurements in the chemistry mode are used. A first validation of the retrieval results in the chemistry mode can be found in Woiwode et al. (2015).

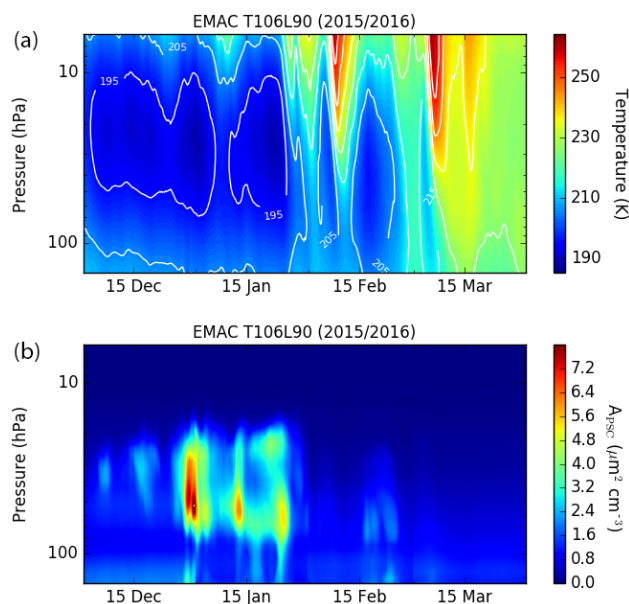


Figure 1. Temporal evolution of temperature (a) and surface area density of PSC particles (liquid plus solid) (b) at northern high latitudes (70–90° N) as a function of pressure during the 2015/2016 Arctic winter, as simulated with EMAC T106L90.

3 The 2015/2016 Arctic winter

3.1 Overview

In the 2015/2016 Arctic winter, temperatures were at record lows from December 2015 to early February 2016 with an unprecedented period of temperatures below the ice formation threshold (Manney and Lawrence, 2016). The extraordinarily strong and cold polar vortex in early winter (November–December 2015) was caused by very low planetary wave activity in the stratosphere (Matthias et al., 2016). The Arctic winter ended in early March by a major final sudden stratospheric warming. By mid-March, the vortex had been displaced far off the pole and split. The offspring vortices decayed rapidly, resulting in a full breakup of the vortex by early April (Manney and Lawrence, 2016).

In Fig. 1, the temporal evolution of temperature and PSC surface area density at high latitudes (70–90° N) as a function of pressure for December 2015 to March 2016 as simulated with EMAC is shown. Temperatures below 195 K are found between 70 and 10 hPa from early December to the end of January. Zonal mean temperatures remained cold afterwards but not as cold as during December and January. Temperatures dropped during the first cold period (December to the end of January) below the ice formation threshold temperatures (Manney and Lawrence, 2016) leading to unprecedented formation of ice PSCs as will be discussed in more detail below (see Fig. 2). The simulated temperatures are in good agreement with observations from Aura/MLS (see Fig. 12 and Sect. 4.1).

The extensive formation of PSCs as simulated with EMAC can be seen in Fig. 1b. Here, the total surface area density (liquid plus solid) is shown. The first PSCs are found in the beginning of December and PSC formation maximises throughout January (between 80 and 20 hPa). During the second cold phase in February, PSCs are still present but to a lesser extent. In Fig. 2, the surface area densities of STS, NAT and ice as a function of pressure are shown (70–90° N). Since the liquid particles have the largest surface area density, A_{STS} is almost identical to A_{PSC} . PSCs consisting of NAT are found between 150 and 20 hPa throughout December and January, and consisting of ice between 80 and 30 hPa in January. Compared to other extreme Arctic winters, e.g. the 2010/2011 winter, much larger amounts of PSCs are simulated in accordance with the preceding low temperatures for the 2015/2016 Arctic winter. Furthermore, the largest surface area density for ice is also simulated for the 2015/2016 Arctic winter as compared to previous Arctic winters, e.g. the 2010/2011 Arctic winter, which has been the most extreme in that respect so far (e.g. Manney et al., 2011; Sinnhuber et al., 2011; Hommel et al., 2014). Ice PSCs persisted in 2015/2016 over a much longer time period than in, e.g. the 2010/2011 Arctic winter, as can be seen in the EMAC results for the 2010/2011 Arctic winter shown in Khosrawi et al. (2017).

3.2 Denitrification

Solid HNO_3 containing PSC particles can sediment out of the stratosphere and thus lead to an irreversible removal of HNO_3 (denitrification). Severe denitrification was observed by Aura/MLS in the 2015/2016 Arctic winter. Figure 3 shows the HNO_3 gas phase distribution as simulated with EMAC for selected dates between 24 December 2015 and 12 February 2016 at 52 hPa. Strong gas phase removal of HNO_3 is evident throughout the entire period considered here. Gas phase HNO_3 is extremely low within the Arctic vortex in December and January, but mixing ratios increase somewhat (but still remain quite low) in February. That this gas phase removal of HNO_3 led to a permanent removal and thus to a denitrification of the stratosphere can be seen from the redistribution of NO_y in the model (Fig. 4).

In model simulations, denitrification can be quantified by applying a passive NO_y^* tracer. Figure 4 shows the simulated NO_y change (ΔNO_y^*) averaged over 70–90° N as a function of pressure and time. The unperturbed NO_y^* was simulated by a passive tracer that was initialised according to the NO_y distribution on 1 December 2015. The passive tracer is transported as all other chemical species but does not undergo any chemical changes or sedimentation. The difference of NO_y and NO_y^* gives the amount of NO_y that has been denitrified/re-nitrified ($\Delta\text{NO}_y = \text{NO}_y - \text{NO}_y^*$).

Figure 4 shows that strong denitrification is also simulated with EMAC for the 2015/2016 Arctic winter. The maximum sequestration is reached at the end of January (about 8 ppbv). Below this layer, re-nitrification (about 4 ppbv) due

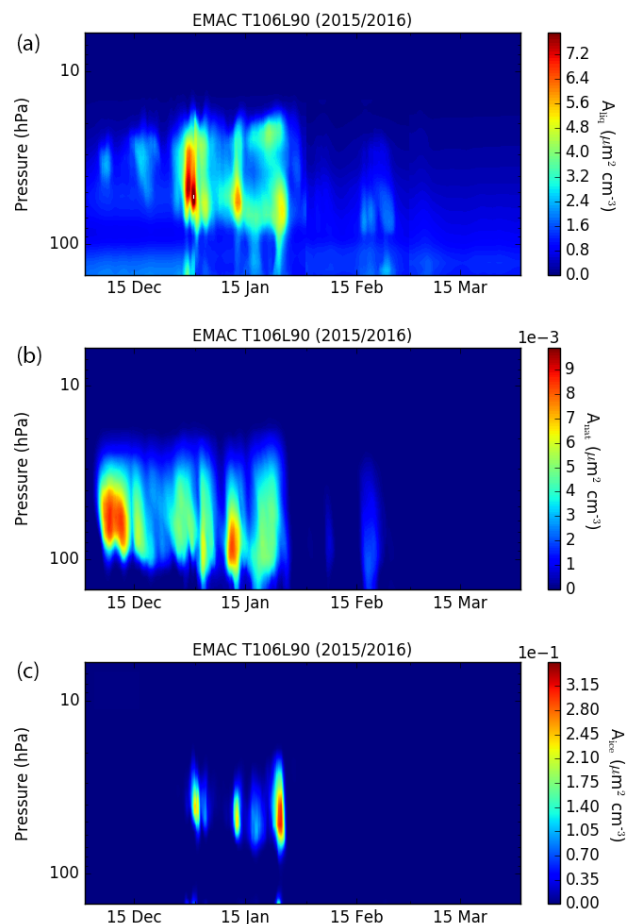


Figure 2. Temporal evolution of surface area density of STS (a), NAT (b) and ice (c) particles at northern high latitudes (70–90° N) as a function of pressure during the 2015/2016 Arctic winter as simulated with EMAC T106L90. Note the differences in the colour bar for A_{liq} ($\mu\text{m}^2 \text{cm}^{-3}$), A_{NAT} ($10^{-3} \mu\text{m}^2 \text{cm}^{-3}$) and A_{ice} ($10^{-1} \mu\text{m}^2 \text{cm}^{-3}$).

to the evaporation of the sedimenting PSC particles at higher pressure levels (lower altitudes) is clearly visible. Thus, the amount of HNO_3 that has been permanently removed (denitrified) is between 4 and 8 ppbv. Diabatic descent within the polar vortex causes the downward shift of the denitrified/re-nitrified areas.

3.3 Dehydration

The long period of temperatures below the ice formation threshold led to much greater dehydration than previously seen in the Arctic (Manney and Lawrence, 2016). Large areas of ice PSC throughout January were observed with CALIPSO that also were the greatest observed in the Arctic in the 8 years of the CALIPSO data record (Voigt et al., 2016). In the EMAC simulation, large areas of ice PSCs are simulated throughout January (Fig. 2c). Dehydration peaks

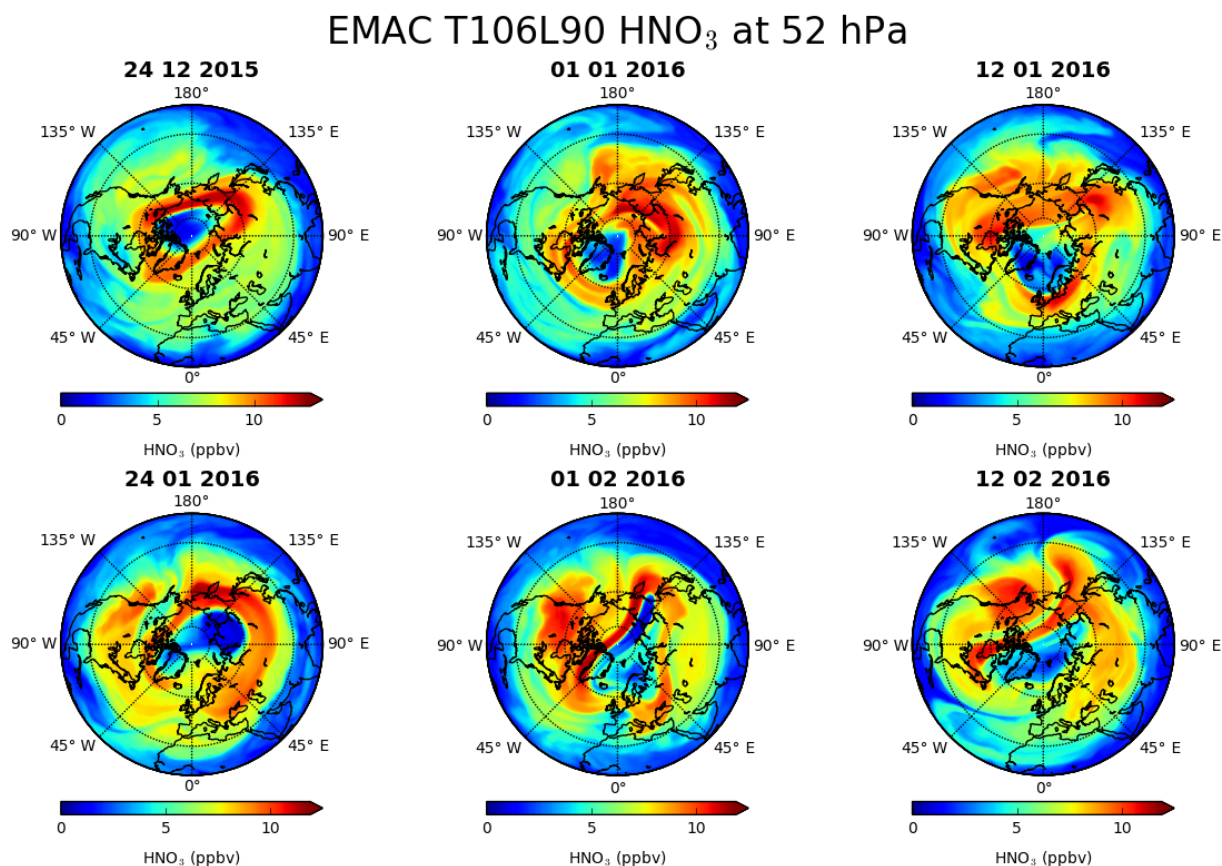


Figure 3. Distribution of HNO₃ as simulated with EMAC T106L90 at 52 hPa on certain dates between 24 December 2015 and 12 February 2016.

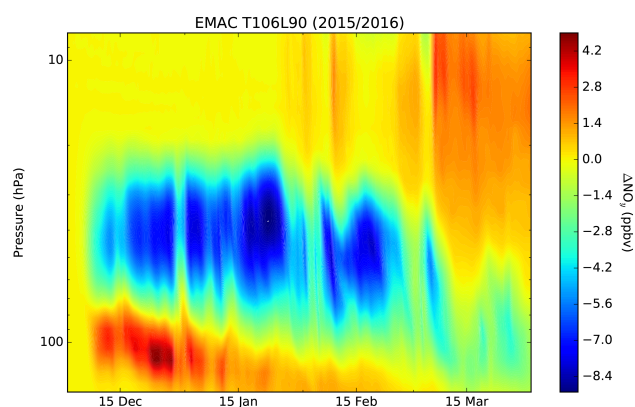


Figure 4. Redistribution of NO_y (ΔNO_y) simulated with EMAC T106L90 (difference of NO_y and the passive tracer NO_y^{*} ($\Delta\text{NO}_y = \text{NO}_y - \text{NO}_y^*$, averaged over 70–90° N).

in the EMAC simulation towards the end of January and is also the strongest simulated dehydration compared to other cold winters, e.g. the 2010/2011 Arctic winter. The simulated dehydration in EMAC is also in agreement with ob-

servations. Trace gas measurements from Aura/MLS show that exceptional dehydration occurred during the 2015/2016 Arctic winter (Manney and Lawrence, 2016).

Figure 5 shows the EMAC H₂O distribution at selected dates during the 2015/2016 winter at 52 hPa. On 24 December 2015, the H₂O distribution shows the usual background H₂O mixing ratios in the Arctic region. From January onwards, mixing ratios drop and an area with mixing ratios below 5 ppmv is found north of Scandinavia. Mixing ratios decrease further throughout January and the area of dehydration increases. From February onwards, H₂O mixing ratios start to increase again but still remain lower than the pre-winter values.

Dehydration from the EMAC simulation is derived by using total “stratospheric” hydrogen ($2\text{CH}_4 + \text{H}_2\text{O}$) as a substitute for a passive H₂O tracer (e.g. Rinsland et al., 1996; Schiller et al., 1996). Molecular hydrogen (H₂) is nearly constant in the lower and middle stratosphere and can therefore be neglected in the calculation of total hydrogen. The quantity $2\text{CH}_4 + \text{H}_2\text{O}$ is generally constant in the stratosphere. However, slight deviations from this quasi-conserved quantity can be found at high latitudes during winter where transport of mesospheric air rich in molecular hydrogen and poor

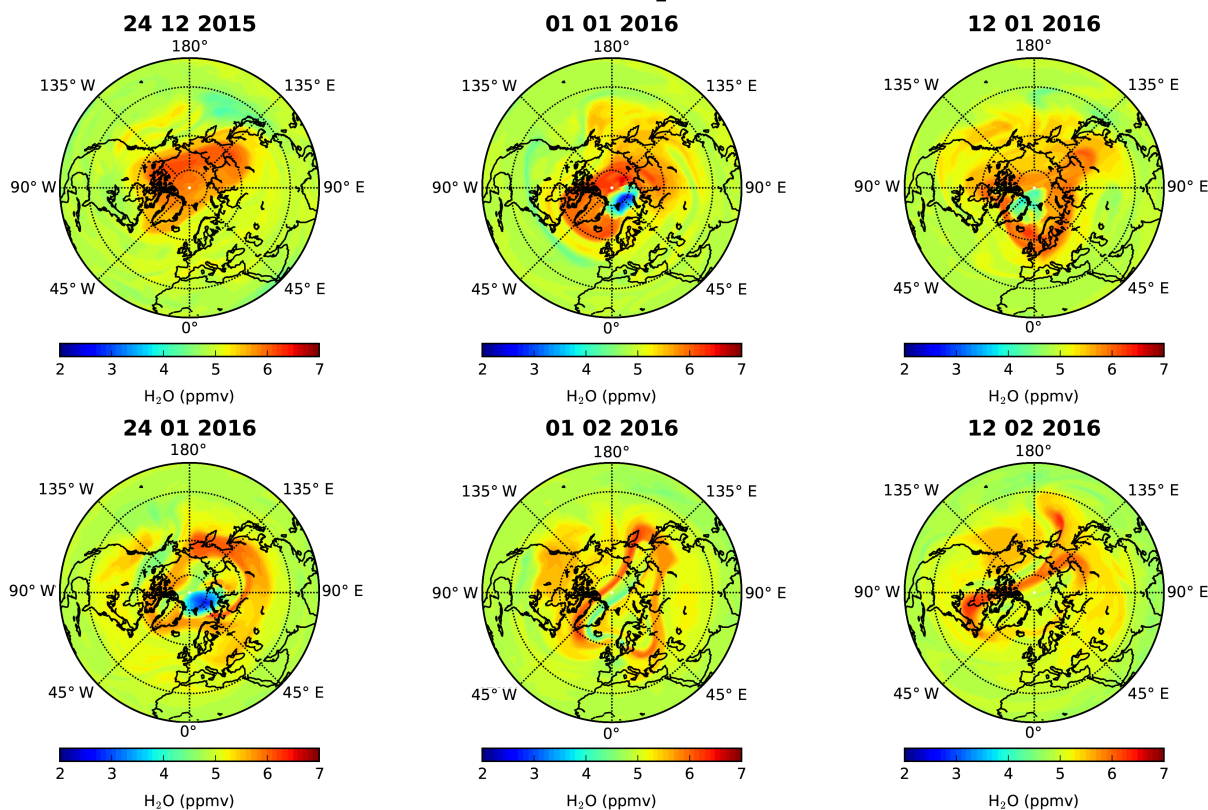
EMAC T106L90 H₂O at 52 hPa

Figure 5. Distribution of H₂O as simulated with EMAC T106L90 at 52 hPa on certain dates between 24 December 2015 and 12 February 2016.

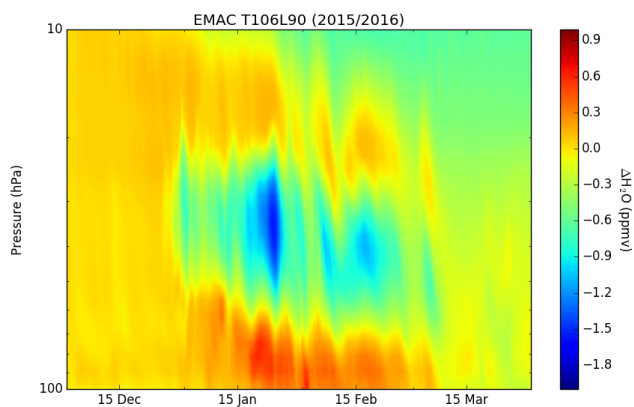


Figure 6. Redistribution of H₂O ($\Delta\text{H}_2\text{O}$) as simulated with EMAC T106L90 at northern high latitudes (70–90° N) as a function of pressure during the 2015/2016 Arctic winter (difference of total hydrogen $2\text{CH}_4 + \text{H}_2\text{O}$ at time t and total hydrogen at time $t_0 = 1$ December ($\Delta\text{H}_2\text{O} = (2\text{CH}_4 + \text{H}_2\text{O})(t) - (2\text{CH}_4 + \text{H}_2\text{O})(t_0)$)).

in water vapour and methane is brought into the upper stratosphere (e.g. LeTexier et al., 1988; Engel et al., 1996).

The change in H₂O ($\Delta\text{H}_2\text{O}$) is calculated by taking the difference of total hydrogen at time t and total hydrogen at time t_0 ($\Delta\text{H}_2\text{O} = (2\text{CH}_4 + \text{H}_2\text{O})(t) - (2\text{CH}_4 + \text{H}_2\text{O})(t_0)$, with $t_0 = 1$ December). The exceptional dehydration during the 2015/2016 Arctic winter can be seen in the temporal evolution of $\Delta\text{H}_2\text{O}$ as a function of pressure averaged over 70–90° N (Fig. 6). The decrease of $\Delta\text{H}_2\text{O}$ throughout January and February shows a H₂O removal of around 1 ppmv extending between 60 and 30 hPa. Sequestration into PSC particles reached its maximum in mid-January ($\Delta\text{H}_2\text{O}$ of up to 2 ppmv). Below the depleted areas, re-hydration (up to 0.6 ppmv) due to the evaporation of the sedimenting PSC particles at higher pressure levels (lower altitudes) is clearly visible. Thus, the amount of H₂O that has been permanently removed (dehydrated) is between 0.6 and 1 ppmv.

3.4 Ozone loss

The 2015/2016 Arctic winter appeared to have the greatest potential seen yet for record Arctic ozone loss (Manney and Lawrence, 2016). Temperatures in the Arctic lower stratosphere were at record lows from December 2015 to early February 2016 (Manney and Lawrence, 2016; Matthias et al.,

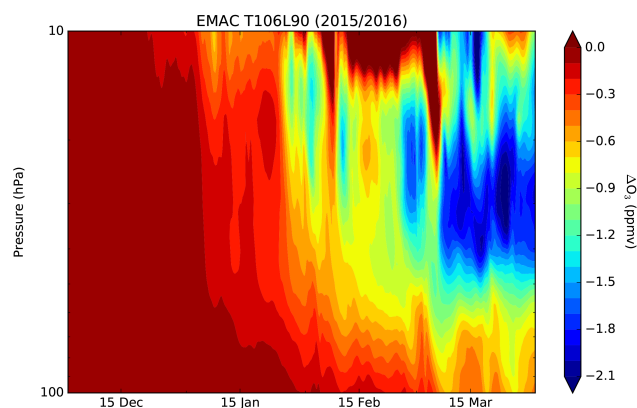


Figure 7. Ozone loss (ΔO_3) as simulated with EMAC T106L90 (difference of O_3 and the passive tracer O_3^* ($\Delta O_3 = O_3 - O_3^*$), averaged over $70\text{--}90^\circ\text{N}$) as a function of time and pressure for the 2015/2016 Arctic winter.

2016). As was shown by Manney and Lawrence (2016), ozone destruction began earlier and proceeded more rapidly than in 2010/2011, the winter that so far has been the one with the strongest observed ozone loss in the Arctic (Manney et al., 2011). The reason that lower-stratospheric ozone loss did not reach the extent of that in spring 2011 was primarily due to a major final stratospheric warming in early March 2016 that led to a vortex split and a full breakdown of the vortex by early April (Manney and Lawrence, 2016).

In the following, the EMAC simulation is used to investigate ozone depletion during the 2015/2016 Arctic winter and compare the results with previous Arctic winters. Ozone depletion (ΔO_3) from the model simulation is determined by the difference between the modelled ozone O_3 and a passive ozone tracer O_3^* ($\Delta O_3 = O_3 - O_3^*$). The passive ozone tracer was initialised on 1 December 2015 according to the ozone distribution on that day and was then advected and mixed as all other chemical species but did not undergo any chemical changes. The simulated ozone depletion (averaged over $70\text{--}90^\circ\text{N}$) is shown in Fig. 7. From mid-January onwards, ozone depletion is visible in the EMAC simulation and a maximum depletion of about 2.1 ppmv is reached at about 30 hPa in mid-March.

The simulated total column ozone loss time series from 1 December to 31 March averaged over $70\text{--}90^\circ\text{N}$ is shown in Fig. 8. Changes in the total column become visible from the end of January onwards. The absolute maximum in total column ozone loss of about 117 DU is reached on 7 March. Note that, rather than employing a vortex-following coordinate, e.g. equivalent latitude, we have not chosen to perform our analysis on a fixed geographic latitude band. Such an approach is justified here because the use of a passive ozone tracer allows dynamical and chemical processes to be separated, thus facilitating the quantification of chemical ozone loss. On equivalent latitudes, the same amount of ozone loss

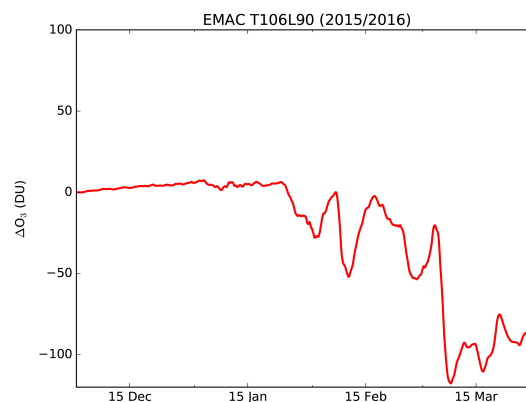


Figure 8. Total column ozone loss (ΔO_3) from EMAC T106L90 ($70\text{--}90^\circ\text{N}$) for the 2015/2016 Arctic winter. Total column loss has been derived from the difference between the active tracer O_3 and the passive tracer O_3^* ($\Delta O_3 = O_3 - O_3^*$).

in terms of mixing ratio is derived, while in terms of column loss ozone loss it is 10 % less (103 DU).

3.5 Comparison to recent Arctic winters

The EMAC T42L90 simulation is used to compare the 2015/2016 Arctic winter to previous Arctic winters. The results from both simulations, T42L90 and T106L90, are quite similar as can be seen from the time series comparison shown in Sect. 4 where the EMAC simulations are compared to Aura/MLS observations. The agreement with the Aura/MLS measurements is slightly better for the T106L90 simulation.

Although considerable ozone loss occurred during the 2015/2016 Arctic winter, ozone loss was not as strong as in 2010/2011 as can be seen from Figs. 9 and 10. In Fig. 9, the March mean O_3 column is shown for the years 2010 to 2016. Very low O_3 column values are found in March 2011. Column values reach 250 DU. In March 2016, however, the O_3 column remains quite high.

Figure 10 shows the Arctic mean column O_3 time series (averaged over $60\text{--}90^\circ\text{N}$) from 1 December to 30 April for the four Arctic winters (2009/2010, 2010/2011, 2013/2014 and 2015/2016). The EMAC Arctic mean column O_3 shows considerable interannual variability. In contrast to the other Arctic winters, very low O_3 is found in 2010/2011. The extreme low O_3 column that we find in the EMAC simulation for the 2010/2011 winter is in agreement with the results from Strahan et al. (2013) and Manney et al. (2011) using observations and model simulations. In 2015/2016, the O_3 column was comparably low in early winter, but from February onwards the O_3 column started to increase significantly due to the disturbances of the Arctic stratosphere by sudden stratospheric warmings. In fact, winters with above-average stratospheric wave activity have a warm, disturbed vortex, while winters with weak wave driving have a cold, long-lasting vortex, with well-known impacts on Arctic March

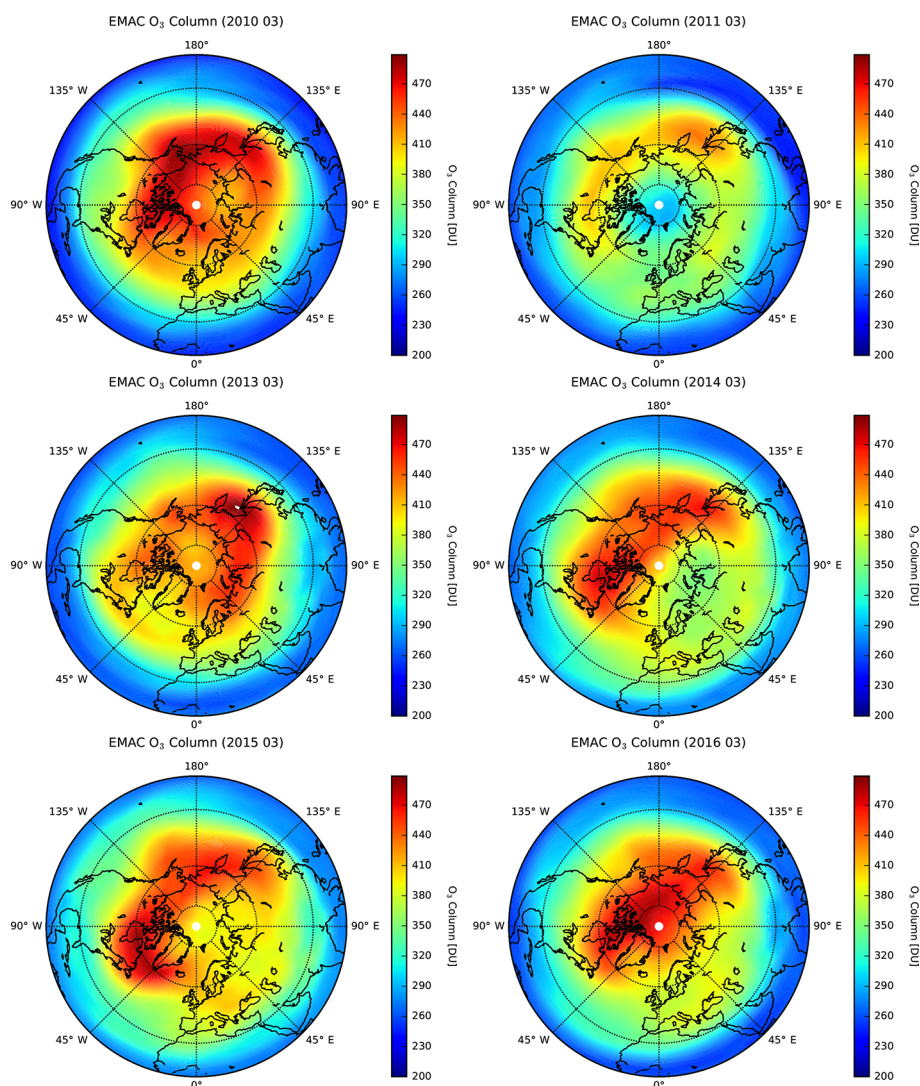


Figure 9. Total ozone column (March monthly mean) from EMAC for the years 2010–2016 (results from the EMAC T42L90 simulation are shown here).

temperatures and O_3 column (Strahan et al., 2013 and references therein). Manney and Lawrence (2016) found from MLS observations that ozone continued to decrease in the vortex at a rate slightly faster than that in 2011 until the beginning of March 2016. However, around mid-March, ozone increased for the rest of the winter, so that the ozone values always remained higher than in 2011. This is also seen in the EMAC simulation. Therefore, our model simulations are in agreement with the results by Manney and Lawrence (2016) who showed that in the 2015/2016 Arctic winter the stratosphere appeared to have the greatest potential seen yet for a massive Arctic ozone loss due to record low temperatures but was disrupted by the final sudden warming in early March. In other words, massive Arctic ozone loss likely would have occurred in the 2015/2016 Arctic winter if the

vortex had remained stable and temperatures remained low into late March.

On the other hand, although ozone loss was not stronger than in 2010/2011, denitrification and dehydration were the strongest observed so far (Manney and Lawrence, 2016). From the EMAC simulation, the same result as from the observations is derived. Figure 11 shows the time series of HNO_3 and H_2O for the same four Arctic winters as shown in Fig. 10. At 48 hPa, several ppbv lower HNO_3 mixing ratios than in previous cold Arctic winters are found from December to February. Pre-winter HNO_3 mixing ratios were around 11 ppbv and drop to 4 ppbv in mid-January. How much lower the H_2O mixing ratios drop due to the dehydration during the 2015/2016 Arctic winter compared to other Arctic winters can be seen in the H_2O time series at 48 hPa (Fig. 11b). In early December, H_2O mixing ratios are as high as 5.8 ppmv

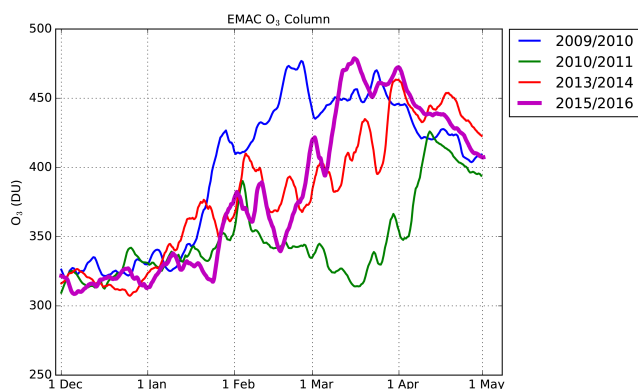


Figure 10. Ozone (O_3) column time series for the 2009/2010 (blue), 2010/2011 (green), 2013/2014 (red) and 2015/2016 (magenta) Arctic winters, averaged over $60\text{--}90^\circ\text{N}$ (results from the EMAC T42L90 simulation are shown here).

and decrease to 5.2 ppmv but decrease for a short period towards the end of January to even lower values (4.7 ppmv). From the end of January, the H_2O mixing ratios increase slowly but still remain lower than the pre-winter values. The H_2O mixing ratios are in addition $\sim 1\text{--}1.5$ ppmv lower in January and February than in previous cold Arctic winters.

4 Comparison to observations

In this study, we compare the EMAC simulations for the 2015/2016 Arctic winter to Aura/MLS observations. In another study (Khosrawi et al., 2017), the EMAC simulations of HNO_3 , temperature and PSC volume density were compared for the 2009/2010 and 2010/2011 Arctic winters with satellite observations (Envisat/MIPAS and Aura/MLS). Here, we consider in addition to temperature and HNO_3 other trace gases such as O_3 , ClO (Sect. 4.1) and H_2O , and compare the simulations to Aura/MLS observations. Additionally, the EMAC simulations are compared to remote sensing observations from GLORIA performed during the POLSTRACC measurement campaign (Sect. 4.2). For the comparisons to Aura/MLS, the EMAC SORBIT output is used (Jöckel et al., 2010), while for the comparison to GLORIA the EMAC global field output is interpolated to the GLORIA measurement geolocations.

4.1 Comparison to Aura/MLS

Figure 12 shows a comparison of the temperature, HNO_3 and O_3 distribution measured by Aura/MLS with the ones simulated with EMAC at about 50 hPa on 15 January 2016. For temperature, as well as for HNO_3 and O_3 , the simulations are in general agreement with the Aura/MLS observations. Nevertheless, some differences are found between model simulations and observations. Temperatures as simulated with EMAC (nudged towards ECMWF operational

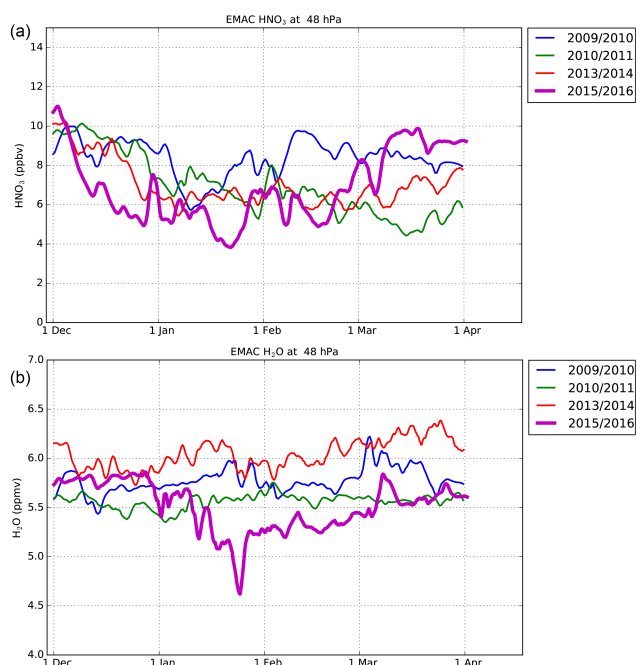


Figure 11. Tracer time series of HNO_3 (a) and H_2O (b) for the 2009/2010 (blue), 2010/2011 (green), 2013/2014 (red) and 2015/2016 (magenta) Arctic winters at 48 hPa, averaged over $70\text{--}90^\circ\text{N}$ (results from the T42L90 simulation are shown here).

analysis) tend to be slightly higher than those measured outside the polar vortex. The trace gas distributions of HNO_3 and O_3 simulated with EMAC show more fine-scale structures, which may be related to the higher horizontal resolution ($1.125^\circ \times 1.125^\circ \sim 125\text{ km} \times 125\text{ km}$ or less depending on latitude) of the EMAC simulation compared to Aura/MLS (measurements every $1.5^\circ \sim 165\text{ km}$ and resolution of $200\text{--}500\text{ km}$ along track). Generally, the simulated HNO_3 mixing ratios are slightly lower than the ones measured with Aura/MLS while the simulated O_3 mixing ratios are quite similar to the observed O_3 .

The temporal development of ClO, HNO_3 and O_3 averaged over $70\text{--}90^\circ\text{N}$ during the 2015/2016 Arctic winter as a function of pressure as simulated with EMAC and observed by Aura/MLS is shown in Fig. 13. Here, the EMAC SORBIT output is used (Jöckel et al., 2010), where EMAC is sampled along the Sun-synchronous orbit of Aura/MLS. The use of the SORBIT output improves the agreement between observations and simulations of trace gases with a diurnal cycle, e.g. ClO, significantly but has a rather minor impact on the comparison between observations and simulations for other trace gases, e.g. O_3 . Generally, the temporal evolution of the trace gas distributions is realistically reproduced in the EMAC simulation. Nevertheless, there are some differences found between measurement and model simulations. In the observations, increased ClO mixing ratios are already found in December,

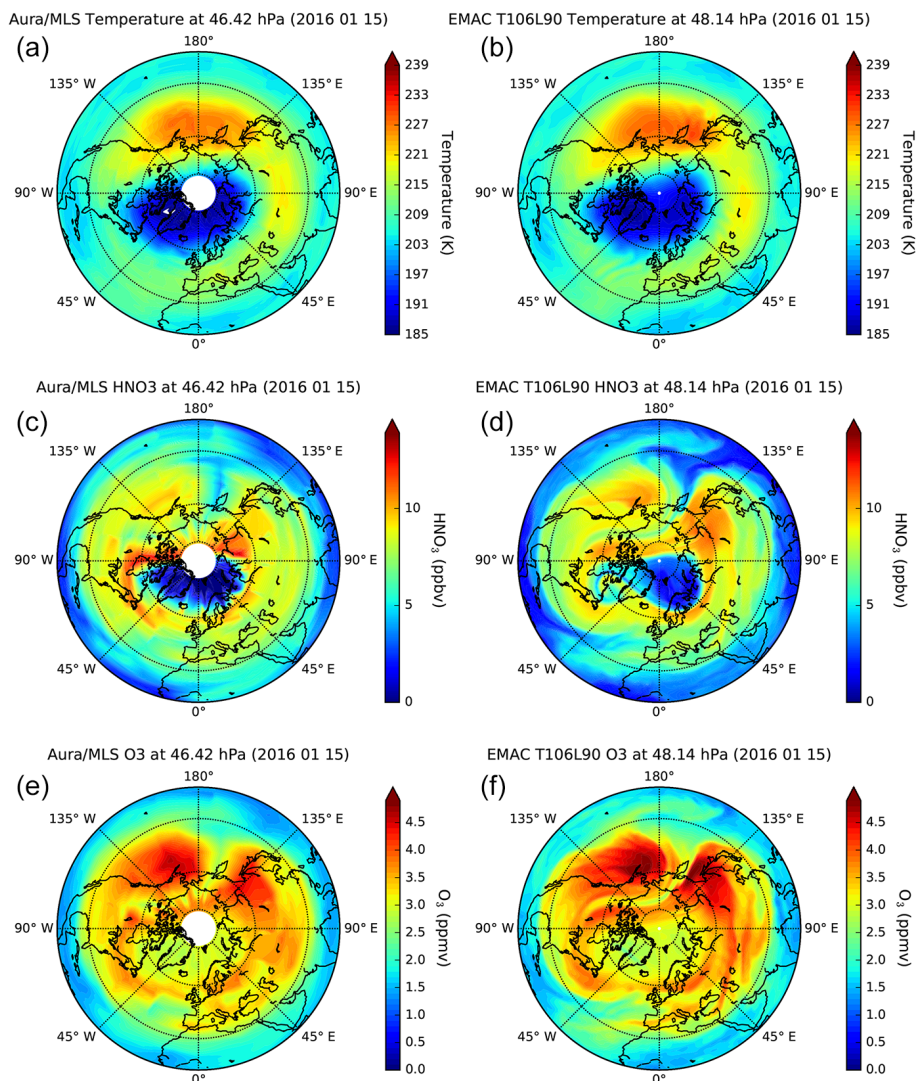


Figure 12. Temperature, HNO_3 and O_3 distribution measured by Aura/MLS (a, c, e) and simulated by EMAC T106L90 (b, d, f) at ~ 50 hPa on 15 January 2016.

whereas in the model simulation the increase of ClO occurs somewhat later. However, the enhancement of ClO_x ($\text{ClO}_x = \text{Cl} + \text{ClO} + \text{HOCl} + \text{OCIO} + 2 \cdot \text{Cl}_2 + 2 \cdot \text{Cl}_2\text{O}_2$) in the EMAC simulation is found at the same time as in the Aura/MLS ClO observation, thus indicating that the later increase in ClO is not necessarily caused by the activation of chlorine being too late in the model simulation but could also be caused by the partitioning between the active chlorine species. In EMAC, the photolysis rates are calculated by the submodel JVAL (Sect. 2.1). JVAL is part of the standard configuration of EMAC that was also used in the EMAC simulations contributing to the Chemistry-Climate Model Initiative (CCMI; Jöckel et al., 2016). An intercomparison of several photolysis schemes has shown that JVAL provides lower photolysis rates at very high solar zenith angles ($> 90^\circ$) for, e.g. Cl_2O_2 , than other schemes. Thus, the partitioning of

chlorine-containing species may be shifted for high solar zenith angles and thus could be the cause for the delay in the activation of ClO in the model simulation. However, to entirely rule out the cause for this difference, further studies are necessary which are beyond the scope of this study. The ClO mixing ratios are maximum in February in both the observations and model simulations. However, at the maximum, higher mixing ratios are found, and these extend over a larger vertical range in the EMAC simulation than in Aura/MLS observations.

The temporal evolution of the HNO_3 distribution as a function of pressure shows that the model simulation captures the general features well. In early December, HNO_3 mixing ratios are slightly underestimated by EMAC (~ 1 ppbv). Gas phase removal of HNO_3 due to uptake in PSCs is more strongly simulated at higher pressure levels (December to

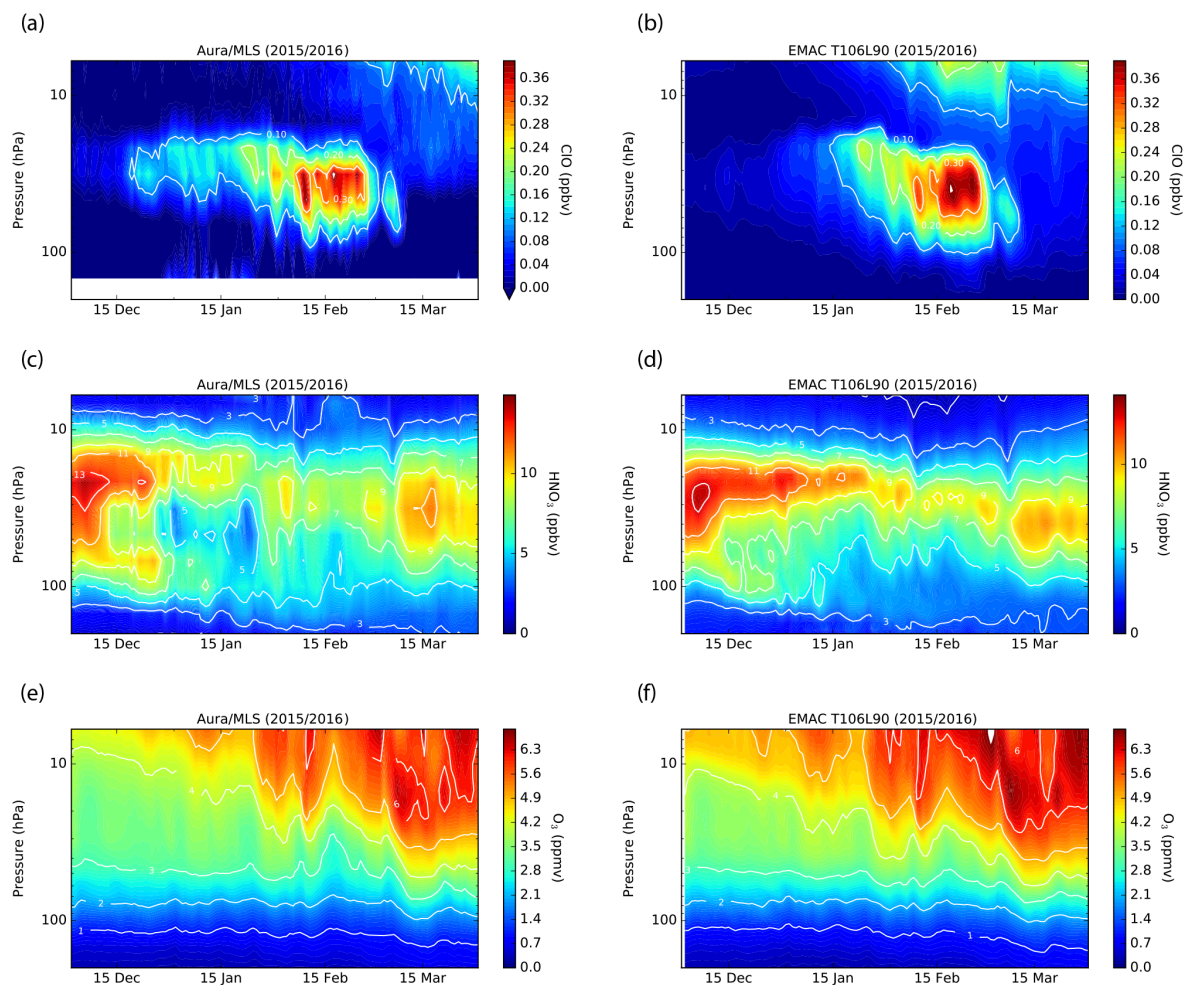


Figure 13. Temporal evolution of daily mean ClO, HNO₃ and O₃ at northern high latitudes (averaged over 70–90° N) as a function of pressure as observed by Aura/MLS (**a**, **c**, **e**) and simulated by EMAC T106L90 (**b**, **d**, **f**) for the 2015/2016 Arctic winter (EMAC SORBIT output used).

January at around 100 hPa) while underestimated at lower pressure levels (January to February at around 50 hPa). PSCs composed of NAT form in EMAC as soon as temperatures drop below $T_{\text{NAT}} - 3$ K, which often results in a too-early formation of NAT particles. Among other things, this has also an impact on the denitrification, as was found in another study comparing EMAC simulations for the 2009/2010 and 2010/2011 Arctic winters with Envisat/MIPAS and Aura/MLS observations (Khosrawi et al., 2017). Because NAT is calculated before STS in the model, the NAT formation occurs at the expense of STS since the available HNO₃ is first consumed by the NAT clouds (e.g. Wohltmann et al., 2013). Since in reality STS and NAT clouds are often observed at the same time (e.g. Pitts et al., 2011; Peter and Groöb, 2012), this could be one explanation for the deviations in the HNO₃ distribution.

The temporal evolution of EMAC O₃ (Fig. 13f) is quite similar to that observed by Aura/MLS (Fig. 13e), especially

in the lower stratosphere. In the upper stratosphere, more O₃ is brought down, leading to higher O₃ in the EMAC simulation above 20 hPa in March compared to Aura/MLS.

Figure 14 shows the time series of HNO₃ and O₃ at 50 hPa for Aura/MLS and the EMAC T42 and T106 simulation. In the EMAC simulation, the HNO₃ is slightly underestimated in the beginning of December (by about 1 ppbv). Larger differences at 50 hPa are found in the time period of denitrification (from the end of December to the end of January). At this time, the EMAC simulations underestimate denitrification at 50 hPa by about 2–3 ppbv. The simulated O₃ is in good agreement with Aura/MLS measurements during December and January. From February onwards, the simulated O₃ is up to 0.25 ppmv higher than the observed O₃. For both species, the T106L90 simulation agrees slightly better with the Aura/MLS observations.

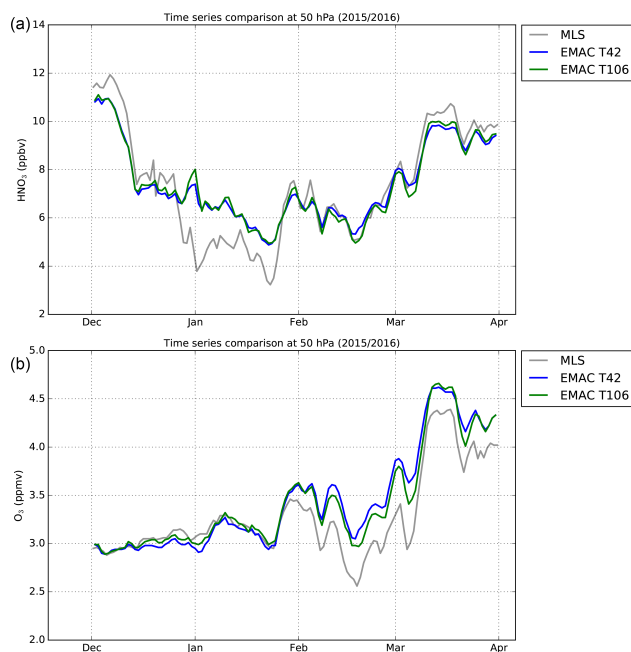


Figure 14. Time series of HNO_3 (a) and O_3 (b) from Aura/MLS measurements (grey) and from the EMAC T42L90 (blue) and EMAC T106L90 (green) at ~ 50 hPa averaged over $70\text{--}90^\circ\text{N}$ (EMAC SORBIT output used).

4.2 Comparison to GLORIA

The EMAC simulations were performed in support of the POLSTRACC campaign. This allows us to evaluate the model performance in the lower stratosphere by comparison to high resolved measurements performed aboard HALO. Here, we show a comparison of EMAC HNO_3 and O_3 to the remote sensing instrument GLORIA. The comparison shown here is for the POLSTRACC flight 21 on 18 March 2016. EMAC output has been taken along the times and locations of GLORIA measurements (Fig. 15). The GLORIA measurements in chemistry mode of flight 21 used in this comparison were performed over Scandinavia. By mid-March, the polar vortex had been displaced off the pole and split. The colder offspring vortex was centred over northern Russia, and during flight 21 air masses at the border of this offspring vortex have been probed.

EMAC HNO_3 and O_3 compares generally well to GLORIA in terms of the distribution and mixing ratios. However, at 12–14 km, the area where the polar vortex has been probed, O_3 mixing ratios from EMAC are slightly lower than the ones observed by GLORIA. The same holds for HNO_3 , but differences between EMAC and GLORIA are larger. The underestimation of polar vortex O_3 in the EMAC simulation could be either caused by a too-weak downward transport or a too-strong ozone destruction in the model. The former reason, however, is more likely, since a well-known feature in EMAC is that the downward transport is underestimated in

the lower parts of the polar vortices (Brühl et al., 2007), despite the model vorticity and divergence fields being nudged towards ECMWF analysis. Further, ozone loss in EMAC is rather underestimated than overestimated as was found in the evaluation study by Khosrawi et al. (2009).

Another difference between EMAC and GLORIA is that less fine-scale structure is simulated with EMAC than observed by GLORIA, which is probably due to the rather coarse horizontal resolution of EMAC (T106 corresponding to $1.125^\circ \times 1.125^\circ$) compared to GLORIA. Nevertheless, these results show that EMAC simulations can be used for comparisons to aircraft measurements. In the future, simulations with EMAC with an even higher horizontal resolution (T255) are anticipated, which are expected to result in even better agreement with observations derived aboard the aircraft. However, it should be kept in mind that a good agreement between model simulations and observations can only be obtained if the model simulations are nudged towards meteorological analysis. It can be expected that comparison with free-running model simulations would show larger differences. Further, the results are also limited by the accuracy of the meteorological analysis; e.g. resolving small-scale temperature fluctuations and mountain waves will still be problematic even when a T255 resolution is used.

5 Conclusions

In this study, an overview of the chemistry and dynamics of the 2015/2016 Arctic winter as simulated with EMAC was given. The EMAC simulations were performed with a T106L90 resolution and nudged toward ECMWF operational analysis. Chemical–dynamical processes such as denitrification, dehydration and ozone loss were investigated, and comparisons to satellite observations by the Aura/MLS as well as to airborne measurements with GLORIA performed aboard HALO were shown.

From the EMAC simulation, we derive a maximum polar stratospheric O_3 loss of ~ 2 ppmv or 117 DU in terms of column in mid-March (averaged over $70\text{--}90^\circ\text{N}$). Note that we did not use equivalent latitudes here since separation between chemical and dynamical processes is achieved via the passive O_3 tracer. On equivalent latitudes, the same amount of ozone loss in terms of mixing ratio is derived, while in terms of column loss ozone loss it is 10 % less (103 DU). The stratosphere was denitrified by about 4–8 ppbv HNO_3 and dehydrated by about 0.6–1 ppmv H_2O from the middle to the end of February. In agreement with the analysis of Aura/MLS observations by Manney and Lawrence (2016), we find that ozone loss was quite strong in 2015/2016 but not as strong as in 2010/2011. Denitrification and dehydration on the other hand were so far the strongest observed in the Arctic stratosphere.

Comparison of trace gas distributions of HNO_3 , ClO and O_3 shows that the EMAC simulations nudged toward

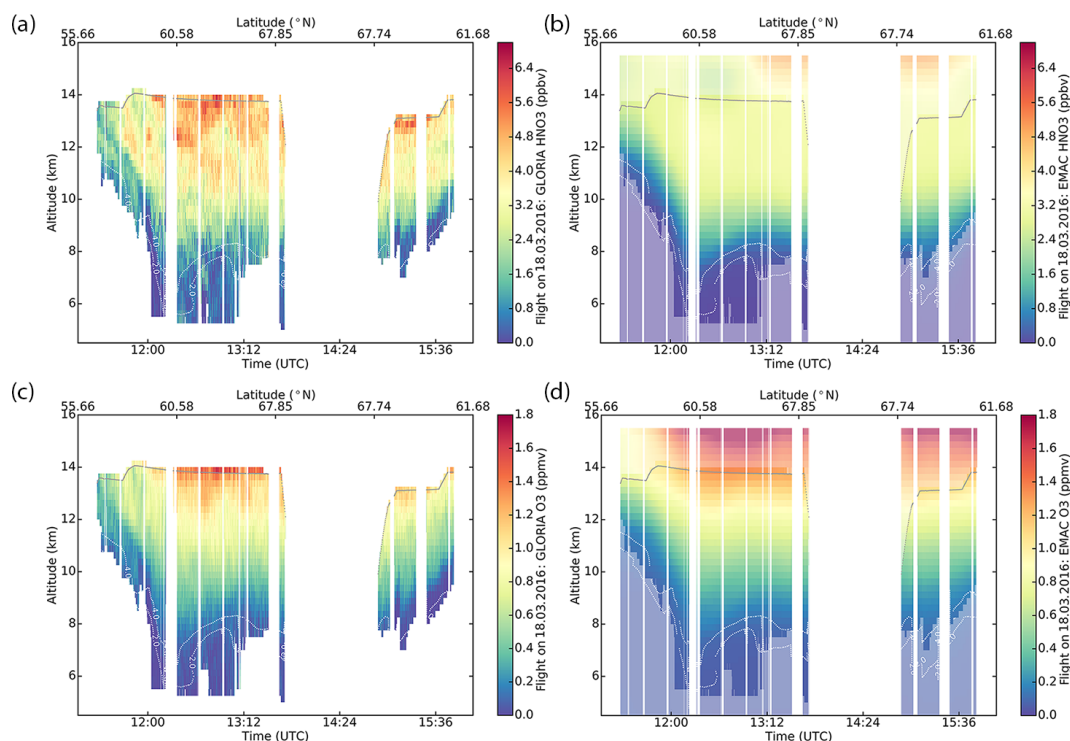


Figure 15. GLORIA HNO₃ and O₃ observations during flight 21 on 18 March 2016 (a, c) and EMAC T106L90 output along the flight track (b, d).

ECMWF operational analysis generally reproduce well the Aura/MLS observations during the 2015/2016 Arctic winter. However, there are some differences between the EMAC simulations and observations which need sensitivity studies in the future to improve the agreement between the model simulations and observations. In the EMAC simulation, HNO₃ is slightly underestimated (by about 1 ppbv). Larger differences are found in the area of denitrification which could be related to the partitioning between STS and NAT in the model. The observed increase in ClO at the beginning of the winter is simulated later with EMAC. Since the enhancement in modelled ClO_x is found roughly at the same time as the observed increase in ClO, the disparity in the behaviour of modelled and measured ClO may arise from chlorine activation being delayed in the model due to inaccuracies in the partitioning between chlorine species at high solar zenith angles.

The comparison to GLORIA measurements shows that EMAC simulations nudged toward ECMWF operational analysis can reproduce the observations. Further, this comparison shows that, though EMAC is a climate model, EMAC simulations can be applied in support of aircraft campaigns and these simulations provide a valuable data set not only for flight analysis but also for measurement–model intercomparisons.

Data availability. Data from the EMAC simulations are available from the authors upon request. MLS data are available at <https://mls.jpl.nasa.gov>.

Competing interests. The authors declare that they have no conflict of interest.

Special issue statement. This article is part of the special issue “The Modular Earth Submodel System (MESSy) (ACP/GMD inter-journal SI)” and “The Polar Stratosphere in a Changing Climate (POLSTRACC) (ACP/AMT inter-journal SI)”. It is not associated with a conference.

Acknowledgements. We would like to thank the European Centre for Medium-Range Weather Forecasts (ECMWF) for providing their meteorological analyses. We also would like to thank the MLS team for providing their data. MLS data were obtained from the NASA Goddard Earth Sciences and Information Center. Work at the Jet Propulsion Laboratory, California Institute of Technology, was done under contract with the National Aeronautics and Space Administration. S. Johansson has received funding from the European Community’s Seventh Framework Programme (FP7/2007–2013) under grant agreement 603557. We would like to thank the GLORIA team for performing the measurements aboard HALO during the POLSTRACC campaign. Atmospheric research with HALO is supported by the Priority

Programme 1294 of the Deutsche Forschungsgemeinschaft. EMAC simulations were performed on the Institute Cluster II at the Steinbuch Center for Computing at Karlsruhe Institute of Technology. We acknowledge support by Deutsche Forschungsgemeinschaft and open-access publishing fund of Karlsruhe Institute of Technology.

The article processing charges for this open-access publication were covered by a Research Centre of the Helmholtz Association.

Edited by: Amanda Maycock

Reviewed by: two anonymous referees

References

- Atkinson, R., Baulch, D. L., Cox, R. A., Crowley, J. N., Hampson, R. F., Hynes, R. G., Jenkin, M. E., Rossi, M. J., and Troe, J.: Evaluated kinetic and photochemical data for atmospheric chemistry: Volume III – gas phase reactions of inorganic halogens, *Atmos. Chem. Phys.*, 7, 981–1191, <https://doi.org/10.5194/acp-7-981-2007>, 2007.
- Brühl, C., Steil, B., Stiller, G., Funke, B., and Jöckel, P.: Nitrogen compounds and ozone in the stratosphere: comparison of MIPAS satellite data with the chemistry climate model ECHAM5/MESSy1, *Atmos. Chem. Phys.*, 7, 5585–5598, <https://doi.org/10.5194/acp-7-5585-2007>, 2007.
- Carslaw, K. S., Luo, B. P., Clegg, S. L., Peter, T., Brimblecombe, P., and Crutzen, P. J.: Stratospheric aerosol growth and HNO_3 gas phase depletion from coupled HNO_3 and water uptake by liquid particles, *Geophys. Res. Lett.*, 21, 2479–2482, 1994.
- Carslaw, K. S., Clegg, S. L., and Brimblecombe, P.: A thermodynamic model of the system $\text{HCl-HNO}_3\text{-H}_2\text{SO}_4\text{-H}_2\text{O}$, including solubilities of HBr, from 328 K to < 200 K, *J. Phys. Chem.*, 99, 11557–11574, 1995.
- Carslaw, K. S., Kettleborough, J., Northway, M. J., Davies, S., Gao, R.-S., Fahey, D. W., Baumgardner, D. G., Chipperfield, M. P., and Kleinböhl, A.: A vortex-wide simulation of the growth and sedimentation of large nitric acid hydrate particles, *J. Geophys. Res.*, 107, 8300, <https://doi.org/10.1029/2001JD000467>, 2002.
- Crutzen, P. J. and Arnold, F.: Nitric acid cloud formation in the cold Antarctic stratosphere: A major cause for the springtime ‘ozone hole’, *Nature*, 342, 651–655, 1986.
- Dee, D. P., Uppala, S. M., Simmons, A. J., Berrisford, P., Poli, P., Kobayashi, S., Andrae, U., Balmaseda, M. A., Balsamo, G., Bauer, P., Bechtold, P., Beljaars, A. C. M., van de Berg, L., Bidlot, J., Bormann, N., Delsol, C., Dragani, R., Fuentes, M., Geer, A. J., Haimberger, L., Healy, S. B., Hersbach, H., Hólm, E. V., Isaksen, I., Kållberg, P., Köhler, M., Matricardi, M., McNally, A. P., Monge-Sanz, B. M., Morcrette, J.-J., Park, B.-K., Peubey, C., deRosnay, P., Tavalato, C., Thépaut, J.-N., and Vitart, F.: The ERA-Interim reanalysis: configuration and performance of the data assimilation system, *Q. J. Roy. Meteorol. Soc.*, 137, 553–597, 2011.
- Dörnbrack, A., Gisinger, S., Pitts, M. C., Poole, L. R., and Matill, M.: Multilevel cloud structures over Svalbard, *Mon. Weather. Rev.*, 145, 1149–1159, <https://doi.org/10.1175/mwr-d-16-0214.1>, 2017.
- Engel, A., Schiller, C., Schmidt, U., Borchers, R., Ovarlez, H., and Ovarlez, J.: The total hydrogen budget in the Arctic winter stratosphere during the European Arctic Stratospheric Ozone Experiment, *J. Geophys. Res.*, 101, 14495–14503, 1996.
- Fahey, D. W., Kelly, K. K., Ferry, G. V., Poole, L. R., Wilson, J. C., Murphy, D. M., Loewenstein, M., and Chan, K. R.: In situ measurements of total reactive nitrogen, total water, and aerosol in a polar stratospheric cloud in the Antarctic, *J. Geophys. Res.*, 94, 11299–11315, 1989.
- Fahey, D. W., Kelly, K. K., Kawa, S. R., Tuck, A. F., Loewenstein, M., Chan, K. R., and Heid, L. E.: Observations of denitrification and dehydration in the winter polar stratosphere, *Nature*, 344, 321–324, 1990.
- Fahey, D. W., Gao, R. S., Carslaw, K. S., Kettleborough, J., Popp, P. J., Northway, M. J., Holecek, J. C., Ciciora, S. C., McLaughlin, R. J., Thompson, T. L., Winkler, R. H., Baumgardner, D. G., Gandrud, B., Wennberg, P. O., Dhaniyala, S., McKinley, K., Peter, T., Salawitch, R. J., Bui, T. P., Elkins, J. W., Webster, C. R., Atlas, E. L., Jost, H., Wilson, J. C., Herman, R. L., Kleinböhl, A., and von König, M.: The detection of large HNO_3 -containing particles in the winter Arctic stratosphere, *Science*, 291, 1026–1031, 2001.
- Friedl-Vallon, F., Gulde, T., Hase, F., Kleinert, A., Kullessa, T., Maucher, G., Neubert, T., Olschewski, F., Piesch, C., Preusse, P., Rongen, H., Sartorius, C., Schneider, H., Schönfeld, A., Tan, V., Bayer, N., Blank, J., Dapp, R., Ebersoldt, A., Fischer, H., Graf, F., Guggenmoser, T., Höpfner, M., Kaufmann, M., Kretschmer, E., Latzko, T., Nordmeyer, H., Oelhaf, H., Orphal, J., Riese, M., Schardt, G., Schillings, J., Sha, M. K., Suminska-Ebersoldt, O., and Ungermann, J.: Instrument concept of the imaging Fourier transform spectrometer GLORIA, *Atmos. Meas. Tech.*, 7, 3565–3577, <https://doi.org/10.5194/amt-7-3565-2014>, 2014.
- Froidevaux, L., Jiang, Y. B., Lambert, A., Livesey, N. J., Read, W. G., Waters, J. W., Browell, E. V., Hair, J. W., Avery, M. A., McGee, T. J., Twigg, L. W., Sumnicht, G. K., Jucks, K. W., Margitan, J. J., Sen, B., Stachnik, R. A., Toon, G. C., Bernath, P. F., Boone, C. D., Walker, K. A., Filipiak, M. J., Harwood, R. S., Fuller, R. A., Manney, G. L., Schwartz, M. J., Daffer, W. H., Drouin, B. J., Cofield, R. E., Cuddy, D. T., Jarnot, R. F., Knosp, B. W., Perun, V. S., Snyder, W. V., Stek, P. C., Thurstans, R. P., and Wagner, P. A.: Validation of Aura Microwave Limb Sounder stratospheric ozone measurements, *J. Geophys. Res.*, 113, D15S20, <https://doi.org/10.1029/2007JD008771>, 2008.
- Fueglistaler, S., Luo, B. P., Voigt, C., Carslaw, K. S., and Peter, T.: NAT-rock formation by mother clouds: a microphysical model study, *Atmos. Chem. Phys.*, 2, 93–98, <https://doi.org/10.5194/acp-2-93-2002>, 2002.
- Hanson, D. R. and Mauersberger, K.: Laboratory studies of the nitric acid trihydrate: Implications for the south polar stratosphere, *Geophys. Res. Lett.*, 15, 855–858, 1988.
- Hommel, R., Eichmann, K.-U., Aschmann, J., Bramstedt, K., Weber, M., von Savigny, C., Richter, A., Rozanov, A., Witrock, F., Khosrawi, F., Bauer, R., and Burrows, J. P.: Chemical ozone loss and ozone mini-hole event during the Arctic winter 2010/2011 as observed by SCIAMACHY and GOME-2, *Atmos. Chem. Phys.*, 14, 3247–3276, <https://doi.org/10.5194/acp-14-3247-2014>, 2014.
- Hoyle, C. R., Engel, I., Luo, B. P., Pitts, M. C., Poole, L. R., Groö, J.-U., and Peter, T.: Heterogeneous formation

- of polar stratospheric clouds – Part 1: Nucleation of nitric acid trihydrate (NAT), *Atmos. Chem. Phys.*, 13, 9577–9595, <https://doi.org/10.5194/acp-13-9577-2013>, 2013.
- Jiang, Y. B., Froidevaux, L., Lambert, A., Livesey, N. J., Read, W. G., Waters, J. W., Bojkov, B., Leblanc, T., McDermid, I. S., Godin-Beekmann, S., Filipiak, M. J., Harwood, R. S., Fuller, R. A., Daffer, W. H., Drouin, B. J., Cofield, R. E., Cuddy, D. T., Jarnot, R. F., Knosp, B. W., Perun, V. S., Schwartz, M. J., Snyder, W. V., Stek, P. C., Thurstans, R. P., Wagner, P. A., Allaart, M., Andersen, S. B., Bodeker, G., Calpini, B., Claude, H., Coetzee, G., Davies, J., De Backer, H., Dier, H., Fujiwara, M., Johnson, B., Kelder, H., Leme, N. P., König-Langlo, G., Kyrö, E., Laneve, G., Fook, L. S., Merrill, J., Morris, G., Newchurch, M., Oltmans, S., Parrondos, M. C., Posny, F., Schmidlin, F., Skrivankova, P., Stubi, R., Thompson, D. T. A., Thouret, V., Vitatte, P., Vömel, H., von Der Gathen, P., Yela, M., and Zabolocki, G.: Validation of Aura Microwave Limb Sounder Ozone by ozonesonde and lidar measurements, *J. Geophys. Res.*, 112, D24S34, <https://doi.org/10.1029/2007JD008776>, 2007.
- Jöckel, P., Kerkweg, A., Pozzer, A., Sander, R., Tost, H., Riede, H., Baumgaertner, A., Gromov, S., and Kern, B.: Development cycle 2 of the Modular Earth Submodel System (MESSy2), *Geosci. Model Dev.*, 3, 717–752, <https://doi.org/10.5194/gmd-3-717-2010>, 2010.
- Jöckel, P., Tost, H., Pozzer, A., Kunze, M., Kirner, O., Brenninkmeijer, C. A. M., Brinkop, S., Cai, D. S., Dyroff, C., Eckstein, J., Frank, F., Garny, H., Gottschaldt, K.-D., Graf, P., Grewe, V., Kerkweg, A., Kern, B., Matthes, S., Mertens, M., Meul, S., Neu-maier, M., Nützel, M., Oberländer-Hayn, S., Ruhnke, R., Runde, T., Sander, R., Scharffe, D., and Zahn, A.: Earth System Chemistry Integrated Modelling (ESCI-Mo) with the Modular Earth Submodel (MESSy, version 2.51), *Geosci. Model Dev.*, 9, 1153–1200, <https://doi.org/10.5194/gmd-9-1153-2016>, 2016.
- Kelly, K. K., Tuck, A. F., Murphy, D. M., Proffitt, M. H., Fahey, D. W., Jones, R. L., McKenna, D. S., Loewenstein, M., Podolske, J. R., Strahan, S. E., Ferry, K. R., Chan, J. F., Vedder, G. V., Gregory, G. L., Hynes, W. D., McCormick, M. P., Browell, E. V., and Heidt, L. E.: Dehydration in the lower Antarctic stratosphere during late winter and early spring, 1987, *J. Geophys. Res.*, 94, 11317–11357, 1989.
- Khaykin, S. M., Engel, I., Vömel, H., Formanyuk, I. M., Kivi, R., Korshunov, L. I., Krämer, M., Lykov, A. D., Meier, S., Naebert, T., Pitts, M. C., Santee, M. L., Spelten, N., Wienhold, F. G., Yushkov, V. A., and Peter, T.: Arctic stratospheric dehydration – Part 1: Unprecedented observation of vertical redistribution of water, *Atmos. Chem. Phys.*, 13, 11503–11517, <https://doi.org/10.5194/acp-13-11503-2013>, 2013.
- Khosrawi, F., Müller, R., Proffitt, M. H., Ruhnke, R., Kirner, O., Jöckel, P., Groß, J.-U., Urban, J., Murtagh, D., and Nakajima, H.: Evaluation of CLaMS, KASIMA and ECHAM5/MESSy1 simulations in the lower stratosphere using observations of Odin/SMR and ILAS/ILAS-II, *Atmos. Chem. Phys.*, 9, 5759–5783, <https://doi.org/10.5194/acp-9-5759-2009>, 2009.
- Khosrawi, F., Kirner, O., Stiller, G., Höpfner, M., Santee, M. L., Kellmann, S., and Braesicke, P.: Comparison of ECHAM5/MESSy Atmospheric Chemistry (EMAC) Simulations of the Arctic winter 2009/2010 and 2010/2011 with Envisat/MIPAS and Aura/MLS Observations, *Atmos. Chem. Phys. Discuss.*, <https://doi.org/10.5194/acp-2017-503>, in review, 2017.
- Kirner, O., Ruhnke, R., Buchholz-Dietsch, J., Jöckel, P., Brühl, C., and Steil, B.: Simulation of polar stratospheric clouds in the chemistry-climate model EMAC via the submodel PSC, *Geosci. Model Dev.*, 4, 169–182, <https://doi.org/10.5194/gmd-4-169-2011>, 2011.
- Kleinert, A., Friedl-Vallon, F., Guggenmoser, T., Höpfner, M., Neubert, T., Ribalda, R., Sha, M. K., Ungermann, J., Blank, J., Ebersoldt, A., Kretschmer, E., Latzko, T., Oelhaf, H., Olschewski, F., and Preusse, P.: Level 0 to 1 processing of the imaging Fourier transform spectrometer GLORIA: generation of radiometrically and spectrally calibrated spectra, *Atmos. Meas. Tech.*, 7, 4167–4184, <https://doi.org/10.5194/amt-7-4167-2014>, 2014.
- Kondo, Y., Irie, H., Koike, M., and Bodeker, G.: Denitrification and nitrification in the Arctic stratosphere during the winter of 1996–1997, *Geophys. Res. Lett.*, 27, 337–340, 2000.
- Koop, T., Biermann, U. M., Raber, W., Luo, B. P., Crutzen, P. J., and Peter, T.: Do stratospheric aerosol droplets freeze above the ice frost point?, *Geophys. Res. Lett.*, 22, 917–920, 1995.
- LeTexier, H., Solomon, S., and Garcia, R. R.: The role of molecular hydrogen and methane oxidation in the water vapour budget of the stratosphere, *Q. J. Roy. Meteorol. Soc.*, 114, 281–295, 1988.
- Livesey, N. J., Filipiak, M. J., Froidevaux, L., Read, W. G., Lambert, A., Santee, M. L., Jiang, J. H., Pumphrey, H. C., Waters, J. W., Cofield, R. E., Cuddy, D. T., Daffer, W. H., Drouin, B. J., Fuller, R. A., Jarnot, R. F., Jiang, Y. B., Knosp, B. W., Li, Q. B., Perun, V. S., Schwartz, M. J., Snyder, W. V., Stek, P. C., Thurstans, R. P., Wagner, P. A., Avery, M., Browell, E. V., Cammas, J.-P., Christensen, L. E., Diskin, G. S., Gao, R.-S., Jost, H.-J., Loewenstein, M., Lopez, J. D., Nedelec, P., Osterman, G. B., Sachse, G. W., and Webster, C. R.: Validation of Aura Microwave Limb Sounder O₃ and CO observations in the upper troposphere and lower stratosphere, *J. Geophys. Res.*, 113, D15S02, <https://doi.org/10.1029/2007JD008805>, 2008.
- Livesey, N. J., Read, W. G., Froidevaux, L., Lambert, A., Manney, G. L., Pumphrey, H. C., Santee, M. L., Schwartz, M. J., Wang, S., Cofield, R. E., Cuddy, D. T., Fuller, R. A., Jarnot, R. F., Jiang, J. H., Knosp, B. W., Stek, P. C., Wagner, P. A., and Wu, D. L.: Aura Microwave Limb Sounder (MLS) Version 3.3 and 3.4 Level 2 data quality and description document, Tech. Rep. JPL D-33509, available at: <http://mls.jpl.nasa.gov/> (last access: 26 October 2017), 2013.
- Livesey, N. J., Santee, M. L., and Manney, G. L.: A Match-based approach to the estimation of polar stratospheric ozone loss using Aura Microwave Limb Sounder observations, *Atmos. Chem. Phys.*, 15, 2015, 9945–9963, <https://doi.org/10.1029/acp-2015-9945-2015>, 2015.
- Livesey, N. J., Read, W. G., Wagner, P. A., Froidevaux, L., Lambert, A., Manney, G. L., Millán Valle, L. F., Pumphrey, H. C., Santee, M. L., Schwartz, M. J., Wang, S., Fuller, R. A., Jarnot, R. F., Knosp, B. W., and Martinez, E.: Aura Microwave Limb Sounder (MLS) Version 4.2x Level 2 data quality and description document, Tech. Rep. JPL D-33509 Rev. C, available at: <http://mls.jpl.nasa.gov/>, last access: 26 October 2017.
- Lowe, D. and MacKenzie, R.: Review: Polar stratospheric cloud microphysics and chemistry, *J. Atmos. Sol.-Terr. Phys.*, 70, 13–40, 2008.
- Manney, G. L. and Lawrence, Z. D.: The major stratospheric final warming in 2016: dispersal of vortex air and termination of Arc-

- tic chemical ozone loss, *Atmos. Chem. Phys.*, 16, 15371–15396, <https://doi.org/10.5194/acp-16-15371-2016>, 2016.
- Manney, G. L., Santee, M. L., Froidevaux, L., Hoppel, K., Livesey, N. J., and Waters, J. W.: EOS MLS observations of ozone loss in the 2004–2005 Arctic winter, *Geophys. Res. Lett.*, 33, L04802, <https://doi.org/10.1029/2005GL024494>, 2006.
- Manney, G. L., Santee, M. L., Rex, M., Livesey, N. L., Pitts, M. C., Veefkind, P., Nash, E. R., Wollmann, I., Lehmann, R., Froidevaux, L., Poole, L. R., Schoeberl, M. R., Haffner, D. P., Davies, J., Dorokhov, V., Gernandt, H., Johnson, B., Kivi, R., Kyrö, E., Larsen, N., Levelt, P. F., Makshtas, A., McElroy, C. T., Nakajima, H., Concepcion Parrondo, M., Tarasick, D. W., von der Gathen, P., Walker, K. A., and Zinoviev, N. S.: Unprecedented Arctic ozone loss in 2011, *Nature*, 478, 469–475, <https://doi.org/10.1038/nature10556>, 2011.
- Marti, J. and Mauersberger, K.: A survey and new measurements of ice vapor pressure temperatures between 170 and 250 K, *Geophys. Res. Lett.*, 20, 363–366, 1993.
- Matthias, V., Dörnbrack, A., and Stober, G.: The extraordinarily strong and cold polar vortex on the early northern winter 2015/16, *Geophys. Res. Lett.*, 43, 12287–12294, <https://doi.org/10.1002/2016GL071676>, 2016.
- Nedoluha, G. E., Bevilacqua, R. M., Hoppel, K. W., Daehler, M., Shettle, E. P., Homstein, J. H., Fromm, M. D., Lumpe, J. D., and Rosenfield, J. E.: POAM III measurements of dehydration in the Antarctic lower stratosphere, *Geophys. Res. Lett.*, 27, 1683–1686, 2000.
- Pan, L. L., Randel, W. J., Nakajima, H., Massie, S. T., Kanazawa, H., Sasano, Y., Sugita, T., Hayashida, S., and Oschepkov, S.: Satellite observation of dehydration in the Arctic polar stratosphere, *Geophys. Res. Lett.*, 29, 1184, <https://doi.org/10.1029/2001GL014147>, 2002.
- Peter, T.: Microphysics and heterogeneous chemistry of polar stratospheric clouds, *Annu. Rev. Phys. Chem.*, 48, 785–822, 1997.
- Peter, T. and Groöf, J.-U.: Chapter 4: Polar stratospheric clouds and sulfate aerosol particles: Microphysics, denitrification and heterogeneous chemistry, in: *Stratospheric Ozone Depletion and Climate*, edited by: Müller, R., RSC Publishing, Cambridge, 108–144, 2012.
- Pitts, M. C., Poole, L. R., Dörnbrack, A., and Thomason, L. W.: The 2009–2010 Arctic polar stratospheric cloud season: a CALIPSO perspective, *Atmos. Chem. Phys.*, 11, 2161–2177, <https://doi.org/10.5194/acp-11-2161-2011>, 2011.
- Rex, M., Harris, N. R. P., von der Gathen, P., Lehmann, R., Braathen, G. O., Reimer, E., Beck, A., Chipperfield, M., Alfier, R., Allaart, M., O'Connor, F., Dier, H., Dorokhov, V., Fast, H., Gil, M., Kyrö, E., Litynska, Z., Mikkelsen, I. S., Molyneux, M., Nakane, H., Notholt, J., Rummukainen, M., Viatte, P., and Wenger, J.: Prolonged stratospheric ozone loss in the 1995/96 Arctic winter, *Nature*, 389, 835–838, 1997.
- Riese, M., Oelhaf, H., Preusse, P., Blank, J., Ern, M., Friedl-Vallon, F., Fischer, H., Guggenmoser, T., Höpfner, M., Hoor, P., Kaufmann, M., Orphal, J., Plöger, F., Spang, R., Suminska-Ebersoldt, O., Ungermann, J., Vogel, B., and Woiwode, W.: Gimballed Limb Observer for Radiance Imaging of the Atmosphere (GLORIA) scientific objectives, *Atmos. Meas. Tech.*, 7, 1915–1928, <https://doi.org/10.5194/amt-7-1915-2014>, 2014.
- Rinsland, C. P., Gunson, M. R., Salawitch, R. J., Newchurch, M. J., Zander, R., Abbas, M. M., Abrams, M. C., Manney, G. L., Michelsen, H. A., Chang, A. Y., and Goldman, A.: ATMOS measurements of $\text{H}_2\text{O} + 2\text{CH}_4$ and total reactive nitrogen in the November 1994 Antarctic stratosphere: Dehydration and denitrification in the vortex, *Geophys. Res. Lett.*, 23, 2397–2400, 1996.
- Roeckner, E., Brokopf, R., Esch, M., Giorgetta, M., Hagemann, S., Koernblueh, L., Manzini, E., Schlese, U., and Schulzweida, U.: Sensitivity of simulated climate to horizontal and vertical resolution in the ECHAM5 atmosphere model, *J. Climate*, 19, 3771–3791, 2006.
- Salawitch, R., Wofsy, S., Gottlieb, E., Lait, L., Newman, P., Schoeberl, M., Loewenstein, M., Podolske, J., Strahan, S., Proffitt, M., Webster, C., May, R., Fahey, D., Baumgardner, D., Dye, J., Wilson, J., Kelly, K., Elkins, J., Chan, K., and Anderson, J.: Chemical loss of ozone in the Arctic polar vortex in the winter of 1991–1992, *Science*, 261, 1146–1154, 1993.
- Sander, R., Baumgaertner, A., Gromov, S., Harder, H., Jöckel, P., Kerkweg, A., Kubistin, D., Regelin, E., Riede, H., Sandu, A., Tarborrelli, D., Tost, H., and Xie, Z.-Q.: The atmospheric chemistry box model CABBA/MECCA-3.0, *Geosci. Model Dev.*, 4, 373–380, <https://doi.org/10.5194/gmd-4-373-2011>, 2011.
- Sander, R., Jöckel, P., Kirner, O., Kunert, A. T., Landgraf, J., and Pozzer, A.: The photolysis module JVAL-14, compatible with the MESSy standard, and the JVal Pre-Processor (JVPP), *Geosci. Model Dev.*, 7, 2653–2662, <https://doi.org/10.5194/gmd-7-2653-2014>, 2014.
- Sander, S. P., Abbatt, J., Barker, J. R., Burkholder, J. B., Friedl, R. R., Golden, D. M., Huie, R. E., Kolb, C. E., Kurylo, M. J., Moortgat, G. K., Orkin, V. L., and Wine, P. H.: Chemical Kinetics and Photochemical Data for Use in Atmospheric Studies, Tech. rep., Evaluation No. 17, JPL Publication 10-6, Jet Propulsion Laboratory, Pasadena, 2011.
- Santee, M. L., Manney, G. L., Livesey, N. J., and Waters, J. W.: UARS Microwave Limb Sounder observations of denitrification and ozone loss in the 2000 Arctic late winter, *Geophys. Res. Lett.*, 27, 3213–3216, <https://doi.org/10.1029/2000GL011738>, 2000.
- Santee, M. L., Lambert, A., Read, W. G., Livesey, N. J., Cofield, R. E., Cuddy, D. T., Daffer, W. H., Drouin, B. J., Froidevaux, L., Fuller, R. A., Jarnot, R. F., Knosp, B. W., Manney, G. L., Perun, V. S., Snyder, W. V., Stek, P. C., Thurstans, R. P., Wagner, P. A., Waters, J. W., Muscari, G., de Zafra, R. L., Dibb, J. E., Fahey, D. W., Popp, P. J., Marcy, T. P., Jucks, K. W., Toon, G. C., Stachnik, R. A., Bernath, P. F., Boone, C. D., Walker, K. A., Urban, J., and Murtagh, D.: Validation of the Aura Microwave Limb Sounder HNO_3 measurements, *J. Geophys. Res.*, 112, D24S40, <https://doi.org/10.1029/2007JD008721>, 2007.
- Santee, M. L., Lambert, A., Read, W. G., Livesey, N. J., Manney, G. L., Cofield, R. E., Cuddy, D. T., Daffer, W. H., Drouin, B. J., Froidevaux, L., Fuller, R. A., Jarnot, R. F., Knosp, B. W., Perun, V. S., Snyder, W. V., Stek, P. C., Thurstans, R. P., Wagner, P. A., Waters, J. W., Connor, B., Urban, J., Murtagh, D., Ricaud, P., Barret, B., Kleinbühl, A., Kuttippurath, J., Küllmann, H., von Hobe, M., Toon, G. C., and Stachnik, R. A.: Validation of the Aura Microwave Limb Sounder ClO measurements, *J. Geophys. Res.*, 113, S522, <https://doi.org/10.1029/2007JD008762>, 2008.
- Schiller, C., Engel, A., Schmidt, U., Borchers, R., and Ovarlez, J.: The partitioning of hydrogen species in the Arctic winter strato-

- sphere: implications on microphysical parameters, *J. Geophys. Res.*, 101, 14489–14493, 1996.
- Schiller, C., Bauer, R., Cairo, F., Deshler, T., Dörnbrack, A., Elkins, J., Engel, A., Flentje, H., Larsen, N., Levin, I., Müller, M., Oltmans, S., Ovarlez, H., Ovarlez, J., Schreiner, J., Strohm, F., Voigt, C., and Vömel, H.: Dehydration in the Arctic stratosphere during the SOLVE/THESEO-2000 campaigns, *J. Geophys. Res.*, 107, 8293, <https://doi.org/10.1029/2001JD000463>, 2002.
- Sinnhuber, B.-M., Stiller, G., Ruhnke, R., von Clarmann, T., and Kellmann, S.: Arctic winter 2010/2011 at the brink of an ozone hole, *Geophys. Res. Lett.*, 38, L24814, <https://doi.org/10.1029/2011GL049784>, 2011.
- Solomon, S.: Stratospheric ozone depletion: A review of concepts and history, *Rev. Geophys.*, 37, 275–316, 1999.
- Solomon, S., Garcia, R. R., Rowland, F. S., and Wuebbles, D. J.: On the depletion of Antarctic ozone, *Nature*, 321, 755–758, 1986.
- Solomon, S., Haskins, J., Ivy, D., and Min, F.: Fundamental differences between Arctic and Antarctic ozone depletion, *P. Natl. Acad. Sci. USA*, 111, 6220–6225, 2014.
- Strahan, S. E., Douglass, A. R., and Newman, P. A.: The contributions of chemistry and transport to low Arctic ozone in March 2011 derived from Aura MLS observations, *J. Geophys. Res.*, 118, 1563–1576, <https://doi.org/10.1002/jgrd.50181>, 2013.
- Tilmes, S., Müller, R., Engel, A., and Russell III, J.: Chemical ozone loss in the Arctic and Antarctic stratosphere between 1992 and 2005, *Geophys. Res. Lett.*, 33, L20812, <https://doi.org/10.1029/2006GL026925>, 2006.
- van den Broek, M. M. P., Williams, J. E., and Bregman, A.: Implementing growth and sedimentation of NAT particles in a global Eulerian model, *Atmos. Chem. Phys.*, 4, 1869–1883, <https://doi.org/10.5194/acp-4-1869-2004>, 2004.
- Voigt, C., Dörnbrack, A., Wirth, M., Groß, S. M., Baumann, R., Ehard, B., Pitts, M. C., Poole, L. R., Sinnhuber, B.-M., and Oelhaf, H.: Widespread persistent polar stratospheric ice clouds in the Arctic, *Atmos. Chem. Phys. Discuss.*, <https://doi.org/10.5194/acp-2016-1082>, in review, 2016.
- Vömel, H., Oltmans, S. J., Hoffmann, D. J., Deshler, T., and Rosen, J. M.: The evolution of the dehydration in the Antarctic stratospheric vortex, *J. Geophys. Res.*, 100, 13919–13926, 1995.
- Vömel, H., Rummukainen, M., Kivi, R., Karhu, J., Turunen, T., Kyrö, E., Rosen, J., Kjørvi, N., and Oltmans, S.: Dehydration and sedimentation of ice particles in the Arctic stratospheric vortex, *Geophys. Res. Lett.*, 24, 798–798, 1997.
- von Hobe, M., Bekki, S., Borrmann, S., Cairo, F., D'Amato, F., Di Donfrancesco, G., Dörnbrack, A., Ebersoldt, A., Ebert, M., Emde, C., Engel, I., Ern, M., Frey, W., Genco, S., Griessbach, S., Groß, J.-U., Gulde, T., Günther, G., Hösen, E., Hoffmann, L., Homonnai, V., Hoyle, C. R., Isaksen, I. S. A., Jackson, D. R., János, I. M., Jones, R. L., Kandler, K., Kalicinsky, C., Keil, A., Khaykin, S. M., Khosrawi, F., Kivi, R., Kuttippurath, J., Laube, J. C., Lefèvre, F., Lehmann, R., Ludmann, S., Luo, B. P., Marchand, M., Meyer, J., Mitev, V., Molleker, S., Müller, R., Oelhaf, H., Olschewski, F., Orsolini, Y., Peter, T., Pfeilsticker, K., Piesch, C., Pitts, M. C., Poole, L. R., Pope, F. D., Ravagnani, F., Rex, M., Riese, M., Röckmann, T., Rognerud, B., Roiger, A., Rolf, C., Santee, M. L., Scheibe, M., Schiller, C., Schlager, H., Siciliani de Cumis, M., Sitnikov, N., Søvde, O. A., Spang, R., Spelten, N., Stordal, F., Suminska-Ebersoldt, O., Ulanovski, A., Ungermann, J., Viciani, S., Volk, C. M., vom Scheidt, M., von der Gathen, P., Walker, K., Wegner, T., Weigel, R., Weinbruch, S., Wetzel, G., Wienhold, F. G., Wohltmann, I., Woiwode, W., Young, I. A. K., Yushkov, V., Zobrist, B., and Strohm, F.: Reconciliation of essential process parameters for an enhanced predictability of Arctic stratospheric ozone loss and its climate interactions (REC-ONCILE): activities and results, *Atmos. Chem. Phys.*, 13, 9233–9268, <https://doi.org/10.5194/acp-13-9233-2013>, 2013.
- Waibel, A. E., Peter, T., Carslaw, K. S., Oelhaf, H., Wetzel, G., Crutzen, P. J., Pöschl, U., Tsias, A., Reimer, E., and Fischer, H.: Arctic ozone loss due to denitrification, *Science*, 283, 2064–2069, 1999.
- Waters, J., Froidevaux, L., Harwood, R. S., Jarnot, R. F., Pickett, H. M., Read, W. G., Siegel, P. H., Cofield, R. E., Filipiak, M. J., Flower, D. A., Holden, J. R., Lau, G. K., Livesey, N. J., Manney, G. L., Pumphrey, H. C., Santee, M. L., Wu, D. L., Cuddy, D. T., Lay, R. R., Loo, M. S., Perun, V. S., Schwartz, M. J., Stek, P. C., Thurstans, R. P., Boynes, M. A., Chandra, K. M., Chavez, M. C., Chen, G. S., Chudasama, B. V., Dodge, R., Fuller, R. A., Girard, M. A., Jiang, J. H., Jiang, Y. B., Knosp, B. W., LaBelle, R. C., Lam, J. C., Lee, K. A., Miller, D., Oswald, J. E., Patel, N. C., Pukala, D. M., Quintero, O., Scaff, D. M., Van Snyder, W., Tope, M. C., Wagner, P. A., and Walch, M. J.: The Earth Observing System Microwave Limb Sounder (EOS MLS) on the Aura satellite, *IEEE T. Geosci. Remote*, 44, 1075–1092, 2006.
- WMO: Scientific assessment of ozone depletion: 2014, Report No. 55, Geneva, 2010.
- Wohltmann, I., Wegner, T., Müller, R., Lehmann, R., Rex, M., Manney, G. L., Santee, M. L., Bernath, P., Suminska-Ebersoldt, O., Strohm, F., von Hobe, M., Volk, C. M., Hösen, E., Ravagnani, F., Ulanovsky, A., and Yushkov, V.: Uncertainties in modelling heterogeneous chemistry and Arctic ozone depletion in the winter 2009/2010, *Atmos. Chem. Phys.*, 13, 3909–3929, <https://doi.org/10.5194/acp-13-3909-2013>, 2013.
- Woiwode, W., Suminska-Ebersoldt, O., Oelhaf, H., Höpfner, M., Belyaev, G. V., Ebersoldt, A., Friedl-Vallon, F., Groß, J.-U., Gulde, T., Kaufmann, M., Kleinert, A., Krämer, M., Kretschmer, E., Kulassa, T., Maucher, G., Neubert, T., Piesch, C., Preusse, P., Riese, M., Rongen, H., Sartorius, C., Schardt, G., Schönfeld, A., Schuettmeyer, D., Sha, M. K., Strohm, F., Ungermann, J., Volk, C. M., and Orphal, J.: Validation of first chemistry mode retrieval results from the new limb-imaging FTS GLORIA with correlative MIPAS-STR observations, *Atmos. Meas. Tech.*, 8, 81–95, <https://doi.org/10.5194/amt-8-81-2015>, 2015.